Hybrid coupling rules for leaderless heterogeneous oscillators: Uniform global asymptotic and finite-time synchronization

Simone Mariano, Riccardo Bertollo, Romain Postoyan, Luca Zaccarian

Hybrid coupling rules for leaderless heterogeneous oscillators: uniform global asymptotic and finite-time synchronization*

S. Mariano[e], R. Bertollo[d], R. Postoyan[a], L. Zaccarian[b,c]

[a]*Université de Lorraine, CNRS, CRAN, F-54000 Nancy, France.*
[b]*Department of Industrial Engineering, University of Trento, Trento, Italy.*
[c]*LAAS-CNRS, Université de Toulouse, CNRS, Toulouse, France.*
[d]*Department of Mechanical Engineering, TU Eindhoven, The Netherlands.*
[e]*Department of Electrical and Electronic Engineering, University of Melbourne, Australia.*

Abstract

We investigate the engineering scenario where the objective is to synchronize heterogeneous oscillators in a distributed fashion. The internal dynamics of each oscillator are general enough to capture their time-varying natural frequency as well as physical couplings and unknown bounded terms. A communication layer is set in place to allow the oscillators to exchange synchronizing coupling actions through a tree-like leaderless network. In particular, we present a class of hybrid coupling rules depending only on local information to ensure uniform global practical or asymptotic synchronization, which is impossible to obtain by using the Kuramoto model customarily used in the literature. We further show that the synchronization set can be made uniformly globally prescribed finite-time stable by selecting the coupling function to be discontinuous at the origin. Novel mathematical tools on non-pathological functions and set-valued Lie derivatives are developed to carry out the stability analysis. The effectiveness of the approach is illustrated in simulations where we apply our synchronizing hybrid coupling rules to models of power grids previously used in the literature.

Keywords: Cyber-physical systems, synchronization, hybrid dynamical systems, multi-agent systems, uniform stability, finite-time stability, Lyapunov methods.

1. Introduction

The Kuramoto model (Kuramoto (1975)) is used in various research fields to describe and analyze the dynamics of a broad family of systems with oscillatory behavior (Acebron et al. (2005)) including neuroscience (Aokii (2015); Tass (2003); Cumin and Unsworth (2007)), chemistry (Forrester (2015)), power networks (Dörfler and Bullo (2012)) and natural sciences (Leonard et al. (2012)), to cite a few (see also (Strogatz (2003))). The many application areas where Kuramoto dynamics emerged from physical considerations motivated a detailed analysis of the synchronization properties of the model, first for the all-to-all connection case (Aeyels and Rogge (2004)), as originally described by Kuramoto, then for a general interconnection layout (Jadbabaie et al. (2004)), with a focus on the derivation of the least conservative lower bound for a stabilizing coupling gain (Jafarpour and Bullo (2019); Chopra and Spong (2009); Dörfler and Bullo (2011)).

Given its simple and accurate description of natural synchronization phenomena, the Kuramoto model has also inspired the design of distributed communication protocols in engineering applications where the coupling function among different agents can be arbitrarily assigned to achieve synchronization, as in the bio-inspired synchronization of moving particles in (Sepulchre et al. (2007)), the synchronized acquisition of oceanographic data from Autonomous Underwater Vehicles (Baldoni et al. (2007)), in clock synchronization (Kiss (2018)), in mobile sensors networks modeled as particles with coupled oscillator dynamics (Paley et al. (2007)), in monotone coupled oscillators (Mauroy and Sepulchre (2012)) or in other engineering applications surveyed in (Dörfler and Bullo (2014)).

While the sinusoidal coupling of Kuramoto models provides a powerful tool to obtain synchronization in coupled networks of oscillators, it also introduces some undesirable properties for engineering applications. For example, when the network comprises oscillators with the same natural frequency, it is now well-known that a system of Kuramoto oscillators admits, in addition to stable equilibria coinciding with the synchronization set, equilibria that are unstable (see, e.g., (Strogatz (2000); Sepulchre et al. (2007))). The downside of this result is that the closer a solution is initialized to an unstable equilibrium, the longer it will take for phase synchronization to arise: we talk of *non-uniform* convergence

*Work supported by the ANR under grant HANDY ANR-18-CE40-0010. Corresponding author S. Mariano. A preliminary version of this work was presented at the 21th IFAC World Congress, Berlin, Germany (Bertollo et al. (2020)).

Email addresses: simone.mariano@unimelb.edu.au (S. Mariano), r.bertollo@tue.nl (R. Bertollo), romain.postoyan@univ-lorraine.fr (R. Postoyan), zaccarian@laas.fr (L. Zaccarian)

(Sepulchre et al. (2007)). Although non-uniform synchronization may naturally characterize certain physical (Oud (2006)) and biological systems, in general, it is not a desirable property for engineering applications. Indeed, the lack of uniformity may induce arbitrarily slow convergence to the attractor set and poor robustness properties (Miller and Pachter (1997)). Secondly, it may occur in the Kuramoto model that the angular phase mismatch between adjacent oscillators remains constant and different from zero indefinitely: in this case we talk of *phase locking* (Aeyels and Rogge (2004)), which hampers the capability to reach asymptotic collective synchronization. Thirdly, in critical applications, finite-time stability, instead of only asymptotic synchronization, may be a mandatory requirement (Polyakov (2011)).

In this work, we investigate the engineering scenario where the goal is to synthesize local coupling rules to synchronize a set of heterogeneous oscillators. We assume the model of the oscillators to be general enough to capture not only their (time-varying) natural frequency but also physical coupling actions and other unknown bounded terms, thus being able to represent, among many possibilities, networks of Kuramoto oscillators with heterogeneous time-varying natural frequencies. Furthermore, without loss of generality, we introduce suitable resets of the oscillators' phase coordinates, so that they are unwrapped to evolve in a compact set, which includes $[-\pi, \pi]$ consistently with their angular nature. Consequently, we define hybrid 2π-unwinding mechanisms to ensure the forward completeness of the oscillating solutions.

To achieve uniform global phase synchronization, thereby overcoming the limitations of Kuramoto models, we equip the oscillators with a leaderless tree-like communication network to locally exchange coupling actions based on local information. This approach has been already exploited in the context of DC microgrids as in, e.g., (Cucuzzella et al. (2018)), or (Giraldo et al. (2019)), for a network of Kuramoto oscillators equipped with a leader. The selection of a tree-like graph, which can always be derived in a distributed way by using the algorithms surveyed in (Pandurangan et al. (2018)), is also not new while addressing a problem of distributed cooperative control: see (Mayhew et al. (2012b)) in the context of hybrid dynamical systems, or (Bai et al. (2011)) and (Alagoz et al. (2012)) for continuous-time networked systems and power grids, respectively. To define the coupling actions, we present novel hybrid coupling rules for which a Lyapunov-based analysis ensures uniform global (practical or asymptotic) phase synchronization. This result overcomes both the lack of uniform convergence and the phase-locking issues characterizing the Kuramoto model (Sepulchre et al. (2007)). Interestingly, we can design the coupling rules in such a way that the network of oscillators behaves like the original Kuramoto models when the oscillators are near phase synchronization. Furthermore, due to the mild properties that we require for our hybrid coupling function, discontinuous selections are allowed, like in (Coraggio et al. (2020)). When the discontinuity is at the origin, we prove finite-time stability properties. In particular, exact synchronization can be reached in a prescribed finite-time (Song et al. (2017)), and convergence is thus independent of the initial conditions. Compared to the related works in (Mauroy and Sepulchre (2012)) and (Wu and Li (2018)), the finite-time stability property we ensure is global and the convergence time can be arbitrarily prescribed, respectively. We resort for this purpose to non-smooth Lyapunov theory, in particular non-pathological Lyapunov functions and set-valued Lie derivatives (Bacciotti and Ceragioli (2003)), for which we provide new results and novel proof techniques that are of independent interest. Due to the possible presence of discontinuities in the coupling function, the stability analysis is carried out by focusing on the regularization of the dynamics, as typically done in the hybrid formalism of (Goebel et al., 2012, Ch. 4). Finally, simulations are provided to illustrate the theoretical guarantees and demonstrate the potential strength of our hybrid theoretical tools to address both first and second-order oscillators modeling generators in power grids considered in (Dörfler and Bullo (2012)).

The recent submission (Bosso et al. (2021a)) (see also (Bosso et al. (2021b))) also uses hybrid tools to obtain uniform global synchronization guarantees in a Kuramoto setting but in a different context, namely for second-order oscillators (where the ω_i's are states rather than external inputs) and, most importantly, for a network with a leader, which significantly changes the setting compared to the leaderless scenario investigated in this work, where no oscillator is insensible to the coupling actions from its neighbours. With respect to the preliminary version of this work in (Bertollo et al. (2020)), we include the next novel elements: relaxed requirements on the coupling function, time-varying, phase-dependent, (possibly) non-identical natural frequencies, generalizing the two-agents theorems of (Bertollo et al. (2020)) to the case of n oscillators in addition to establishing a set of new stability results missing in (Bertollo et al. (2020)) (finite-time, practical properties and other ancillary results).

The rest of the paper is organized as follows. Notation and background material are given in Section 2. The local hybrid coupling rules and oscillators network model are derived in Section 3. In Section 4, we introduce the regularized version of the dynamics presented in Section 3. In Section 5, we present Lyapunov-based analysis tools establishing the asymptotic properties of our model, while prescribed finite-time results are given in Section 6. Numerical illustrations are provided in Section 7, while most of the technical aspects of our proofs requiring non-smooth analysis concepts are gathered in Section 8. A few proofs of minor importance are relegated to the Appendix.

2. Preliminaries

Notation. Let $\mathbb{R} := (-\infty, \infty)$, $\mathbb{R}_{\geq 0} := [0, \infty)$, $\mathbb{R}_{>0} := (0, \infty)$, $\mathbb{Z}_{\geq 0} := \{0, 1, \dots\}$, $\mathbb{Z}_{>0} := \{1, 2, \dots\}$ and $\mathbb{Z}_{>1} := \{2, \dots\}$. The notation $\mathbb{R}^n$ denotes the n-dimensional Euclidean space with $n \in \mathbb{Z}_{>0}$ and e_i is the i-th element of the natural base of $\mathbb{R}^n$, with $i \in \{1, \dots, n\}$. The notation $\mathbb{B}_n$ denotes the closed unit ball of $\mathbb{R}^n$ centered at the origin and we write $\mathbb{B}$ when its dimension is clear from the context. We

denote with $\emptyset$ the *empty set*. Given a vector $x \in \mathbb{R}^n$, we denote with x_ℓ its ℓ-th element, with $\ell \in \{1,\dots,n\}$, $|x|$ is its Euclidean norm and $|x|_1$ is its 1-norm. The notation $\mathbf{0}_n$ denotes a vector whose $n \in \mathbb{Z}_{>0}$ elements are all equal to 0. The notation $\mathbf{1}_n$ denotes a vector whose $n \in \mathbb{Z}_{>0}$ elements are all equal to 1. Given two vectors $x_1 \in \mathbb{R}^n$ and $x_2 \in \mathbb{R}^m$, we denote $(x_1, x_2) := [x_1^\top x_2^\top]^\top$. Given a matrix $A \in \mathbb{R}^{n\times m}$, $[A]_\ell$ stands for its ℓ-th column and $(A)_s$ for its s-th row, where $\ell \in \{1,\dots,m\}$ and $s \in \{1,\dots,n\}$. Given a vector $x \in \mathbb{R}^n$ and a non-empty set $\mathscr{A} \subset \mathbb{R}^n$ with $n \in \mathbb{Z}_{>0}$, $|x|_{\mathscr{A}} := \inf\{|x-y| : y \in \mathscr{A}\}$ is the distance of x to $\mathscr{A}$. Given a set $\mathscr{S} \subset \mathbb{R}^n$, $\mathrm{cl}(\mathscr{S})$ stands for its closure, $\partial\mathscr{S}$ is its boundary, $\mathrm{int}(\mathscr{S})$ is its interior and $\overline{\mathrm{co}}\,\mathscr{S}$ is its closed convex hull. Given a finite set $\mathscr{S} \subset \mathbb{R}^n$, $|\mathscr{S}|$ denotes its cardinal number. A function $f : \mathbb{R}^n \to \mathbb{R}_{\geq 0}$ is radially unbounded if $f(x) \to \infty$ as $|x| \to \infty$. Let $f : \mathbb{R}^n \to \mathbb{R}$ and $r \in \mathbb{R}$, we denote by $f(r)^{-1}$ the set $\{x \in \mathbb{R}^n : f(x) = r\}$. Let X and Y two non-empty sets, $T : X \rightrightarrows Y$ denotes a *set-valued* map from X to Y. We define the set-valued map sign : $\mathbb{R} \rightrightarrows \{-1, 1\}$ as $\mathrm{sign}(z) = -1$ when $z < 0$, $\mathrm{sign}(z) = 1$ when $z > 0$ and $\mathrm{sign}(0) = \{-1, 1\}$. We refer to class $\mathscr{K}$, $\mathscr{K}_\infty$ and $\mathscr{KL}$ functions as defined in (Goebel et al., 2012, Chap. 3). A function $f : \mathbb{R} \to \mathbb{R}$ is *piecewise continuous* if for any given interval $[a, b]$, with $a < b \in \mathbb{R}$, there exist a finite number of points $a \leq x_0 < x_1 < x_2 < \cdots < x_{k-1} < x_k \leq b$, with $k \in \mathbb{Z}_{\geq 0}$ such that f is continuous on (x_{i-1}, x_i) for any $i \in \{1,\dots,k\}$ and its one-sided limits exist as finite numbers. A function $f : \mathbb{R} \to \mathbb{R}$ is *piecewise continuously differentiable* if for any given interval $[a, b]$, with $a < b \in \mathbb{R}$, there exists a finite number of points $a \leq x_0 < x_1 < x_2 < \cdots < x_{k-1} < x_k \leq b$, with $k \in \mathbb{Z}_{\geq 0}$ such that f is continuous, f is continuously differentiable on (x_{i-1}, x_i) for any $i \in \{1,\dots,k\}$ and its one-sided limits of the difference quotient exist as finite numbers. We define with $\mathrm{uni}([a, b])$ the continuous uniform distribution over the compact interval $[a, b]$ with $a < b \in \mathbb{R}$.

Background on graph theory. We denote an unweighted undirected graph as $\mathscr{G}_u = (\mathscr{V}, \mathscr{E}_u)$, where $\mathscr{V}$ is the set of vertices, or nodes, and $\mathscr{E}_u \subseteq \mathscr{V} \times \mathscr{V}$ is the set of edges, or arcs, composed by unordered pairs of nodes. If a pair (i, j) of nodes belongs to $\mathscr{E}_u$, we say that those nodes are *adjacent* and that j is a *neighbour* of i and vice versa. Given two nodes x and y of an undirected graph $\mathscr{G}_u$, we define as *path* from x to y a set of vertices starting with x and ending with y, such that consecutive vertices are adjacent. If there is a path between any couple of nodes, the graph is called *connected*, otherwise it is called *disconnected*. We define as *subgraph* of $\mathscr{G}_u$ a graph $\mathscr{G}_s = (\mathscr{V}_s, \mathscr{E}_s)$, where $\mathscr{V}_s \subset \mathscr{V}$ and $\mathscr{E}_s \subset \mathscr{E}_u$. An induced subgraph of $\mathscr{G}_u$ that is maximal, subject to be connected, is called a *connected component* of $\mathscr{G}_u$. A *cycle* is a connected graph where every vertex has exactly two neighbours. An acyclic graph is a graph for which no subgraph is a cycle. A connected acyclic graph is called a *tree*.

We denote an unweighted directed graph as $\mathscr{G} = (\mathscr{V}, \mathscr{E})$, where $\mathscr{E} \subseteq \mathscr{V} \times \mathscr{V}$ is composed of ordered pairs, therefore arcs have a specific direction. An arc going from node i to node j is denoted by $(i, j) \in \mathscr{E}$. If a directed graph $\mathscr{G}$ is obtained choosing an arbitrary direction for the edges of an undirected graph $\mathscr{G}_u$, we call it an *oriented* graph, and we say that $\mathscr{G}$ is obtained from an orientation of $\mathscr{G}_u$. If $(i, j) \in \mathscr{E}$, we say that i belongs to the set of *in-neighbors* $\mathscr{I}_j$ of j, while j belongs to the set of *out-neighbors* $\mathscr{O}_i$ of i. The union of $\mathscr{I}_i$ and $\mathscr{O}_i$ gives the more generic set of neighbors $\mathscr{V}_i := \mathscr{I}_i \cup \mathscr{O}_i$ of node i, containing all the nodes connected to it, in any direction. With $B \in \mathbb{R}^{n\times m}$ we denote the incidence matrix of graph $\mathscr{G}$ such that each column $[B]_\ell$, $\ell \in \{1,\dots,m\}$, is associated to an edge $(i, j) \in \mathscr{E}$, and all entries of $[B]_\ell$ are zero except for $b_{i\ell} = -1$ (the tail of edge ℓ) and $b_{j\ell} = 1$ (the head of edge ℓ), namely $[B]_\ell = e_j - e_i$.

3. Oscillators with hybrid coupling

3.1. Flow dynamics

Consider a networked system of n heterogeneous oscillators. To achieve synchronization, the oscillators locally exchange coupling actions through the *unweighted undirected tree*[1] $\mathscr{G}_u := (\mathscr{V}, \mathscr{E}_u)$ made of n nodes and thus $m = n - 1$ edges, $n \in \mathbb{Z}_{>1}$. We assign an arbitrary orientation to $\mathscr{G}_u$, which leads to the oriented tree $\mathscr{G} = (\mathscr{V}, \mathscr{E})$. In this scenario, the oscillator phase corresponding to node i, with $i \in \mathscr{V}$, is denoted θ_i and has the next flow dynamics

$$\dot{\theta}_i = \omega_i(\theta, \mathrm{t}) + \kappa \sum_{j\in\mathscr{O}_i} \sigma(\theta_j - \theta_i + 2q_{ij}\pi) - \kappa \sum_{j\in\mathscr{I}_i} \sigma(\theta_i - \theta_j + 2q_{ji}\pi), \quad (\theta, q) \in C \tag{1}$$

where $\omega_i(\theta, \mathrm{t})$ is a possibly an unknown term modeling the dynamics of the i-th oscillator, which can capture physical coupling actions, its time-varying natural frequency, and any other unknown bounded dynamics affecting the oscillator; see Section 7 for a numerical example. We assume that ω_i is locally bounded, measurable in t, piecewise continuous in θ and such that $\omega_i(\theta, \mathrm{t}) \in \Omega := [\omega_\mathrm{m}, \omega_\mathrm{M}]$ for any time $\mathrm{t} \geq 0$ and $(\theta, q) \in C$, with $\omega_\mathrm{m} \leq \omega_\mathrm{M} \in \mathbb{R}$, namely Ω is a compact interval of values[2]. Since (1) possibly has a discontinuous right-hand side, the notion of solution should be carefully defined, and we postpone this discussion to Section 4 (where we also prove the existence of solutions) to avoid overloading the exposition. For now it suffices to say that a function θ is a solution of (1) if it is absolutely continuous (i.e., it coincides with the integral of its derivative) and satisfies (1) almost everywhere.

Phase θ_i in (1) evolves in the set $[-\pi - \delta, \pi + \delta]$, with $\delta \in (0, \pi)$, which thus covers the unit circle corresponding to

[1] As mentioned in the introduction, we can obtain a spanning tree using any of the distributed, finite-time algorithms described in (Pandurangan et al. (2018)).

[2] The assumption that ω_i, for any $i \in \mathscr{V}$, takes values in the compact set Ω could be relaxed by only assuming boundedness of the mismatch $\sup_{(\mathrm{t},\theta)\in\mathbb{R}_{\geq 0}\times[-\pi-\delta,\pi+\delta]} |\omega_i(\mathrm{t}, \theta) - \omega_j(\mathrm{t}, \theta)|$ for any pair $(i, j) \in \mathscr{E}$, and adapting the proofs accordingly.

phases taking values in $[-\pi,\pi]$. Parameter $\delta>0$ inflates the set of angles $[-\pi,\pi]$ to rule out Zeno solutions as explained in the following, see Section 3.3. Thus, δ is a regularization parameter chosen to be the same for each oscillator. Variable q_{ij}, with $(i,j)\in\mathscr{E}$, is a logic state taking values in $\{-1,0,1\}$, which is constant during flows. Its role is to unwind the difference between the two phases θ_j and θ_i through jumps. Indeed, since θ_j and θ_i are angles, to evaluate their mismatch, loosely speaking, we have to consider their minimum mismatch modulo 2π: q_{ij} is introduced for this purpose as clarified in Section 3.2. The vectors θ and q collect all the states θ_i, $i\in\mathscr{V}$, and q_{ij}, $(i,j)\in\mathscr{E}$, respectively, as formalized in the following, together with the formal definition of the flow set C, namely a compact subset of the state-space where the solutions are allowed to evolve continuously. The gain $\kappa\in\mathbb{R}_{>0}$ is associated with the intensity of each coupling action and it is the same for each interconnection. Finally, the coupling action between each pair of nodes $(i,j)\in\mathscr{E}$ is defined as $\sigma(\theta_j-\theta_i+2q_{ij}\pi)$, where σ is the function used to penalize the phase mismatch $\theta_j-\theta_i+2q_{ij}\pi$ between phases θ_j and θ_i, and it satisfies the next property.

Property 1. *Function σ is piecewise continuous on* $\operatorname{dom}\sigma:=[-\pi-\delta,\pi+\delta]$ *and satisfies*

a) $\sigma(s)=-\sigma(-s)$ *for any* $s\in\operatorname{dom}\sigma$,

b) there exists $\alpha\in\mathscr{K}$ *such that* $\operatorname{sign}(s)\sigma(s)\geq\alpha(|s|)$ *for any* $s\in\operatorname{dom}\sigma\setminus\{0\}$. □

Item a) of Property 1 ensures that σ is an odd function and thus implies $\sigma(0)=0$, while item b) of Property 1 guarantees that $\sigma(s)$ can only be zero at $s=0$. Notice that the sine function, customarily used in the classical Kuramoto model, satisfies item a) but not item b) of Property 1, which is fundamental to establish the global uniform stability result of this work. Examples of functions σ satisfying Property 1 are depicted in Figure 1, together with the sine function for the sake of comparison. We emphasize that the mild assumptions of Property 1 allow considering, among others, intuitive discontinuous selections such as the sign function of Figure 1, which leads to an interesting parallel between (1) and the ternary controllers considered in (De Persis and Frasca (2013)). Another possible example of σ enjoying Property 1 is $\sigma(s)=\sin(s)+u(s)$, where u is such that items a) and b) of Property 1 hold. Note that when u is negligible compared to sin in a neighborhood of the origin, the model behaves locally like the classical Kuramoto network. Also, Property 1 comes with no loss of generality as we consider the scenario where we have the freedom to design the coupling rules among the oscillators and thus σ.

Function σ is only defined on $\operatorname{dom}\sigma=[-\pi-\delta,\pi+\delta]$ according to Property 1. We ensure in the sequel that the argument of σ in (1), namely $\theta_j-\theta_i+2q_{ij}\pi$, belongs to $\operatorname{dom}\sigma$ for all $(i,j)\in\mathscr{E}$, whenever $x\in C$, so that (1) is well-defined, see Section 3.2.

Collecting in the vector $\boldsymbol{\sigma}(x)\in\mathbb{R}^m$ all the coupling actions $\sigma(\theta_j-\theta_i+2q_{ij}\pi)$, with $(i,j)\in\mathscr{E}$, using the same order as the columns of B, the flow dynamics in (1) is written as

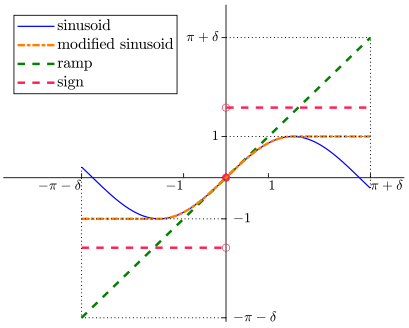

Figure 1: Examples of functions σ satisfying Property 1, together with the sine function (which does not satisfy Property 1).

$$\dot{x}=\begin{bmatrix}\dot{\theta}\\ \dot{q}\end{bmatrix}=f(x,\boldsymbol{\omega}(\theta,t)):=\begin{bmatrix}\boldsymbol{\omega}(\theta,t)-B\kappa\boldsymbol{\sigma}(x)\\ \mathbf{0}_m\end{bmatrix},\quad x\in C, \tag{2}$$

with $\theta:=(\theta_1,\dots,\theta_n)\in[-\pi-\delta,\pi+\delta]^n$, $\boldsymbol{\omega}(\theta,t):=(\omega_1(\theta,t),\dots,\omega_n(\theta,t))\in\Omega^n$, and where $q\in\{-1,0,1\}^m$ is the vector stacking all the q_{ij}'s for $(i,j)\in\mathscr{E}$, ordered as in $\boldsymbol{\sigma}(x)$. Thus, the overall state $x:=(\theta,q)$ evolves in the compact state space defined as

$$X:=[-\pi-\delta,\pi+\delta]^n\times\{-1,0,1\}^m. \tag{3}$$

The flow set C in (2) will be selected as the closed complement of the jump set D introduced next.

3.2. Jump dynamics

We introduce jump rules to constrain each phase θ_i to take values in $[-\pi-\delta,\pi+\delta]$ as well as to guarantee that the argument $\theta_j-\theta_i+2q_{ij}\pi$ of σ in (1) belongs to $\operatorname{dom}\sigma=[-\pi-\delta,\pi+\delta]$ when flowing. To guarantee the latter property, define, for any $(i,j)\in\mathscr{E}$, the jump set

$$D_{ij}:=\left\{x\in X:|\theta_j-\theta_i+2q_{ij}\pi|\geq\pi+\delta\right\}, \tag{4a}$$

and the associated difference inclusion

$$x^+=\begin{bmatrix}\theta^+\\ q^+\end{bmatrix}\in G_{ij}^{\text{ext}}(x):=\begin{bmatrix}\theta\\ G_{ij}(x)\end{bmatrix},\qquad x\in D_{ij}, \tag{4b}$$

where the entries of $G_{ij}:X\rightrightarrows\{-1,0,1\}^m$ are given by

$$(G_{ij})_{(u,v)}:=\begin{cases}\underset{h\in\{-1,0,1\}}{\operatorname{argmin}}\ |\theta_j-\theta_i+2h\pi|, & \text{if } (u,v)=(i,j),\\ \{q_{uv}\}, & \text{otherwise,}\end{cases} \tag{4c}$$

with $(u,v),(i,j)\in\mathscr{E}$. Set D_{ij} in (4a) enforces a jump when $\theta_j-\theta_i+2q_{ij}\pi$ is not in $\operatorname{dom}\sigma$ for $(i,j)\in\mathscr{E}$. Across a jump, according to (4b), only q_{ij} changes in such a way that $|\theta_j-\theta_i+2q_{ij}\pi|<\pi+\delta$ after a jump as formalized in the next lemma whose proof is given in Appendix A to avoid breaking the flow of the exposition.

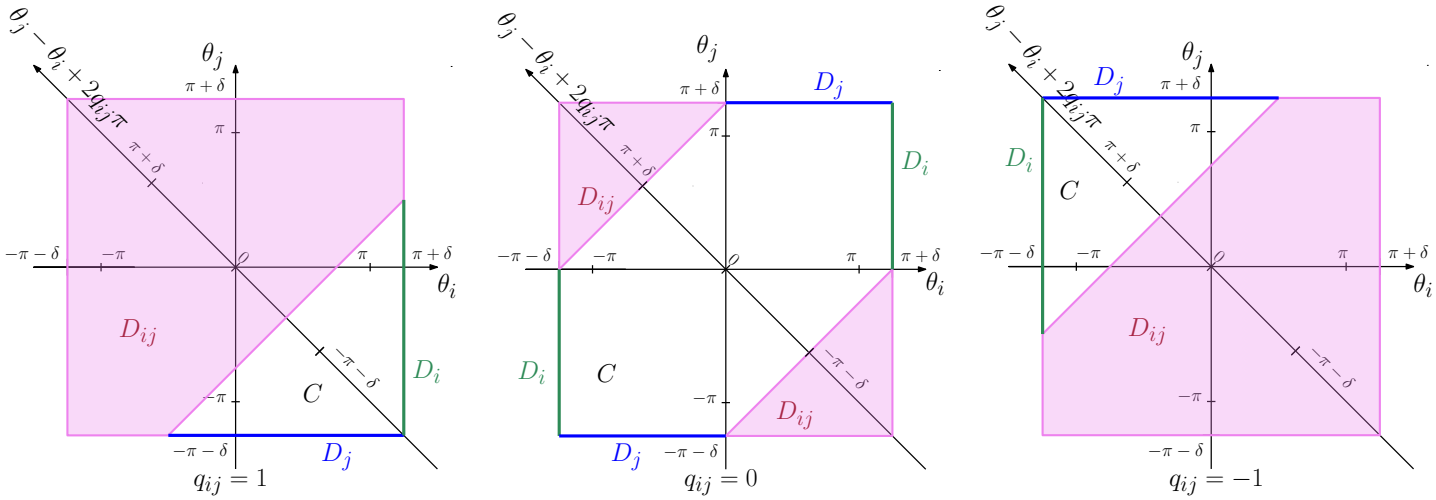

Figure 2: Projection of the flow and jump sets on (θ_i, θ_j) for each value of q_{ij}.

Lemma 1. *For any $(i,j) \in \mathcal{E}$ and $x \in D_{ij}$, any $x^+ \in G_{ij}^{\text{ext}}(x)$ as per* (4b) *satisfies $x^+ \in X$ and $|\theta_j^+ - \theta_i^+ + 2q_{ij}^+\pi| < \pi + \delta$.* □

A second jump rule is introduced for when one of the oscillators $i \in \mathcal{V}$ reaches $|\theta_i| = \pi + \delta$. In this case, a jump of 2π is enforced so that the phase then belongs to $(-\pi - \delta, \pi + \delta)$ while remaining the same modulo 2π. We define for this purpose

$$x^+ = \begin{bmatrix} \theta^+ \\ q^+ \end{bmatrix} = g_i(x) := \begin{bmatrix} g_{i,\theta}(x) \\ g_{i,q}(x) \end{bmatrix}, \qquad x \in D_i, \tag{5a}$$

where the entries of $g_{i,\theta} : X \to [-\pi - \delta, \pi + \delta]^n$ and $g_{i,q} : X \to \{-1, 0, 1\}^m$ are defined as

$$(g_{i,\theta})_j := \begin{cases} \theta_i - \text{sign}(\theta_i)2\pi, & \text{if } j = i, \\ \theta_j, & \text{otherwise,} \end{cases} \tag{5b}$$

$$(g_{i,q})_{(u,v)} := \begin{cases} q_{uv} + \text{sign}(\theta_i), & \text{if } v = i, \\ q_{uv} - \text{sign}(\theta_i), & \text{if } u = i, \\ q_{uv}, & \text{otherwise,} \end{cases} \tag{5c}$$

with $j \in \mathcal{V}$ and $(u,v) \in \mathcal{E}$. The set D_i, $i \in \mathcal{V}$, is defined as

$$D_i := \text{cl}\big(\{x \in X : x \notin D_{uv} \text{ for any } (u,v) \in \mathcal{E}, \text{ and } |\theta_i| = \pi + \delta\}\big). \tag{5d}$$

In view of (5d), the jump rule (5a) is allowed when both $|\theta_i| = \pi + \delta$ and x is not in the interior of D_{uv} for any $(u,v) \in \mathcal{E}$, where a jump may occur according to (4).

Note that each function g_i is continuous on its (not connected) domain because D_i does not contain points with $\theta_i = 0$ for any $i \in \mathcal{V}$.

Finally, switching/jumping ruled by (5) unwinds the phase θ_i without changing the phase mismatches between neighbours, defined as $(\theta_j - \theta_i + 2q_{ij})$, as shown in the next lemma, whose proof is given in Appendix A.

Lemma 2. *For each $i \in \mathcal{V}$ and $x \in D_i$, $x^+ = g_i(x)$ implies $x^+ \in X$ and, for all $(u,v) \in \mathcal{E}$,*

$$\begin{cases} \theta_v^+ - \theta_u^+ + 2q_{uv}^+\pi = \theta_v - \theta_u + 2q_{uv}\pi, \\ |\theta_i^+| = \pi - \delta < \pi + \delta. \end{cases} \tag{6}$$

□

3.3. Overall model

In view of Sections 3.1-B, the overall hybrid model is given by

$$\begin{cases} \dot{x} = f(x, \boldsymbol{\omega}(t)), & x \in C, \\ x^+ \in G(x), & x \in D, \end{cases} \tag{7a}$$

where f is defined in (2), and using (4a) and (5d),

$$D := \Big(\bigcup_{i=1}^{n} D_i\Big) \cup \Big(\bigcup_{(i,j)\in\mathcal{E}} D_{ij}\Big), \tag{7b}$$

$$C = \text{cl}(X \setminus D), \tag{7c}$$

with X defined in (3). The set-valued jump map G is defined in terms of its graph, which is given by

$$\text{gph } G := \Big(\bigcup_{i=1}^{n} \text{gph } g_i\Big) \cup \Big(\bigcup_{(i,j)\in\mathcal{E}} \text{gph } G_{ij}^{\text{ext}}\Big), \tag{7d}$$

with g_i and G_{ij}^{ext} as per (4b), (5a)-(5c). Figure 2 shows three projections of the state space X on the plane (θ_i, θ_j) for some $(i,j) \in \mathcal{E}$, which corresponds to a union of three squares, one for each value of q_{ij}.

Remark 1. Since we envision engineering applications, each phase θ_i with $i \in \mathcal{V}$ may be reconstructed from the angular measurements provided by sensors. Due to the wide variety of outputs provided by commercial sensors, a relevant task is to extrapolate a continuous measurement from a sensor that may return values whose wrapping around 2π is unknown; see, for example, (Reigosa et al. (2018)) and (Anandan and George (2017)). In this scenario, we can implement an algorithm to extract a continuous measurement of

the phase satisfying (2). In particular, following a rationale similar to that proposed in (Mayhew et al., 2012a, Figure 1) for a setting with sampled measurements, we may continuously update an estimate $\theta_{i,e}$ of θ_i. Indeed, for each sensor output $\theta_{i,so}$, we may extract the lifted measurement as the closest one to $\theta_{i,e}$ when performing 2π-wraps $\theta_{i,e}^+ = \theta_{i,so} + 2\pi \operatorname*{argmin}_{h\in\{-1,0,1\}} |\theta_{i,so} - \theta_{i,e} + 2h\pi|$. This rule parallels the selection of (15) and (27b) of (Mayhew et al. (2012a)) for the simpler case of $\mathbb{S}^1$ and scalar angular measurements. □

4. Regularized hybrid dynamics

Model (7) is a time-varying hybrid system with a possibly discontinuous right-hand side, due to the mild properties of σ, see Property 1. Hence, solutions may be understood in the generalized sense of (Goebel et al. (2012)). We consider for this purpose the regularization of (7), so that stability properties for the regularized system carry over to the nominal and generalized solutions of (7). In particular, following (Goebel et al., 2012, Page 79) we consider

$$\begin{cases} \dot{x} \in F(x), & x \in C, \\ x^+ \in G(x), & x \in D, \end{cases} \tag{8a}$$

where C, D, and G coincide with those in (7), and the set-valued map F regularizes f in (2) as

$$F(x) := \begin{bmatrix} \widehat{\Omega} - B\kappa\widehat{\Sigma}(x) \\ \mathbf{0}_m \end{bmatrix}, \quad \forall x \in X, \tag{8b}$$

with the sets $\widehat{\Omega} := \Omega \times \cdots \times \Omega = [\omega_{\mathrm{m}}, \omega_{\mathrm{M}}]^n$ and $\widehat{\Sigma}$ being the Krasovskii regularization of the function $\boldsymbol{\sigma}$ in (2), see for more details (Hájek, 1979, Page 4). More specifically, following (Goebel et al., 2012, Def. 4.13), $\widehat{\Sigma}(x) := \bigcap_{s>0} \overline{\mathrm{co}}\, \boldsymbol{\sigma}((x + s\mathbb{B}) \cap C)$. It is readily verified that, denoting by $\widehat{\sigma}$ the Krasovskii regularization of the scalar function σ, namely

$$\widehat{\sigma}(\tilde{\theta}) := \bigcap_{s>0} \overline{\mathrm{co}}\, \sigma([\tilde{\theta} - s, \tilde{\theta} + s] \cap [-\pi - \delta, \pi + \delta]), \tag{9}$$

for any $\tilde{\theta} \in [-\pi - \delta, \pi + \delta]$, then the set-valued map $\widehat{\Sigma}(x)$ is the stacking (with the same ordering as in $\boldsymbol{\sigma}$) of the set-valued maps $\widehat{\sigma}_{ij}$ defined as

$$\widehat{\sigma}_{ij} := \widehat{\sigma}(\tilde{\theta}_{ij}), \qquad \tilde{\theta}_{ij} := \theta_j - \theta_i + 2q_{ij}\pi, \tag{10}$$

for all $(i, j) \in \mathscr{E}$.

Since the jump set, flow set, and jump map of hybrid system (8) coincide with those of (7), and for any $x \in X$ and $\boldsymbol{\omega} \in \widehat{\Omega}$, $f(x, \boldsymbol{\omega}) \in F(x)$, we study the stability properties of solutions of (7) by concentrating on the regularized dynamics (8). In addition to clarifying the nature of solutions of (7), which may, among other things, present sliding behavior (see Section 6), the advantage of using (8) instead of (7) is that (8) satisfies the so-called hybrid basic conditions (Goebel et al., 2012, As. 6.5), which ensure its well-posedness (Goebel et al., 2012, Thm. 6.30).

Lemma 3. *System* (8) *satisfies the hybrid basic conditions (HBC) of (Goebel et al., 2012, As. 6.5).* □

Proof: Sets C and D, as defined in (4a), (5d), (7b), (7c) are closed, as required by (Goebel et al., 2012, As. 6.5 (A1)). On the other hand, F is the Krasovskii regularization of a function, which satisfies the HBC in view of its locally boundedness on C and (Goebel et al., 2012, Lemma 5.16) as shown in (Goebel et al., 2012, Ex. 6.6), thus (Goebel et al., 2012, As. 6.5 (A2)) is satisfied. Lastly, each g_i and G_{ij}^{ext} has a closed graph, and so due to (7d) the graph of G is closed as well. As consequence, according to (Goebel et al., 2012, Lemma 5.10), G is outer semicontinuous and it is also locally bounded relative to D, thereby satisfying (Goebel et al., 2012, As. 6.5 (A3)). ■

Among other useful properties, Lemma 3 guarantees intrinsic robustness of the stability property established later in Sections 5 and 6, see (Goebel et al., 2012, Ch. 7). To conclude this section, we note that all maximal solutions to (8) are complete[3] and exhibit a (uniform) average dwell-time property, thereby excluding Zeno phenomena. We emphasize that, through Lemmas 1 and 2, the parameter δ plays a key role in establishing that no complete discrete solution exists. In particular, the fact that $\delta \neq 0$ and $\delta \neq \pi$ is key for being able to exclude Zeno solutions.

Proposition 1. *All solutions to* (8) *enjoy a uniform average dwell-time property. Namely, there exist* $\tau_D \in \mathbb{R}_{>0}$ *and* $J_0 \in \mathbb{Z}_{\geq 0}$ *such that, for any solution* x *to* (8) *and for any pair of hybrid times such that* $\mathfrak{t} + \mathfrak{j} \geq \mathfrak{s} + \mathfrak{r}$ *with* $(\mathfrak{s}, \mathfrak{r}), (\mathfrak{t}, \mathfrak{j}) \in \operatorname{dom} x$, $\frac{1}{\tau_D}(\mathfrak{t} - \mathfrak{s}) + J_0 \geq (\mathfrak{j} - \mathfrak{r})$. *Moreover, if* x *is maximal, then it is* $\mathfrak{t}$*-complete, i.e.,* $\sup_{\mathfrak{t}} \operatorname{dom} x = \sup\{\mathfrak{t} \in \mathbb{R}_{\geq 0} : \exists \mathfrak{j} \in \mathbb{Z}_{\geq 0}, (\mathfrak{t}, \mathfrak{j}) \in \operatorname{dom} x\} = +\infty$. □

Proof: We first recall that, in view of Lemma 2, for any $i \in \mathscr{V}$, $x \in D_i$ and $x^+ = g_i(x)$

$$|\theta_i^+| = \pi - \delta < \pi + \delta, \tag{11}$$

while the other θ_j, $j \neq i \in \mathscr{V}$ remain unchanged across such a jump and so does $\theta_j - \theta_i + 2q_{ij}\pi$ for all $(i, j) \in \mathscr{E}$. We also recall that, from Lemma 1, for any $(i, j) \in \mathscr{E}$, $x \in D_{ij}$ and $x^+ \in G_{ij}^{\mathrm{ext}}(x)$

$$|\theta_j^+ - \theta_i^+ + 2q_{ij}^+\pi| \leq \max(2\delta, \pi) < \pi + \delta, \tag{12}$$

while the θ_u and the other $\theta_h - \theta_k + 2q_{hk}\pi$ remain unchanged for any $u \in \mathscr{V}$ and $(h, k) \neq (i, j) \in \mathscr{E}$. From uniform global boundedness of the right hand-side $F(x)$ of the flow dynamics (a consequence of the local boundedness of F and of the boundedness of X), all solutions satisfy a global Lipschitz property with respect to the flowing time and (11) and (12) imply a uniform average dwell time on the jumps from $\bigcup_{i=1}^{n} D_i$

[3] A solution to a hybrid system $\mathscr{H}$ is *maximal* if it cannot be extended and it is *complete* if its domain is unbounded.

and $\bigcup_{(i,j)\in\mathscr{E}} D_{ij}$, respectively. Finally, the uniform average dwell time property of solutions jumping from D derives directly from Lemma 2 and (4b)-(4c). Indeed, (4b)-(4c) imply that jumping from D_{ij} does not affect the triggering condition in D_u or D_{hk}, for any $u \in \mathscr{V}$ and $(i,j) \neq (h,k) \in \mathscr{E}$. In a similar way, Lemma 2 implies that jumping from D_i does not affect the triggering condition in D_j or D_{ij} or D_{ji}, for any $j \neq i \in \mathscr{V}$ and $(i,j) \in \mathscr{E}$ or $(j,i) \in \mathscr{E}$. Thus, a uniform average dwell time on jumps from D stems from the global Lipschitz property of the solutions with respect to the flowing time, along with (11) and (12).

We now check that maximal solutions of (8) are complete by proving that the conditions of (Goebel et al., 2012, Prop. 6.10) hold. First, consider $\xi \in C \setminus D$. Because $\partial C \subset D$, then $\xi \in \text{int}(C)$. Therefore, there exists a neighbourhood U of ξ such that $U \subset C \setminus D$. Thus, for any $x \in U \subset C \setminus D$, the tangent cone[4] to C at x is $T_C(x) = \mathbb{R}^n \times \{0\}^m$. Hence, any $\psi \in F(x)$ in (8b) satisfies $\{\psi\} \cap T_C(x) = \{\psi\} \neq \emptyset$, so that (Goebel et al., 2012, Prop. 6.10 (VC)) holds for any $\xi \in C \setminus D$. On the other hand, the state space X in (3) is bounded, thus item (b) in (Goebel et al., 2012, Prop. 6.10) is excluded. To rule out item (c) in (Goebel et al., 2012, Prop. 6.10), from Lemmas 1 and 2, we have $G(D) \subset X = C \cup D$. Hence, we can apply (Goebel et al., 2012, Prop. 6.10) to conclude that all maximal solutions are complete, thus obtaining t-completeness of solutions in view of their uniform average dwell time property established above. ■

5. Asymptotic stability properties

5.1. Synchronization set and its stability property

To analyze the synchronization properties of system (8), consider the set

$$\mathscr{A} := \{x \in X : \theta_i = \theta_j + 2q_{ij}\pi,\ \forall (i,j) \in \mathscr{E}\}. \tag{13}$$

Because the network is a tree, for any $x \in \mathscr{A}$, the phases θ_i and θ_j coincide modulo 2π not only for any $(i,j) \in \mathscr{E}$ but also for any $i \in \mathscr{V}$ and $j \in \mathscr{V} \setminus \{i\}$. In other words, when $x \in \mathscr{A}$, all the oscillators are synchronized even if they do not share a direct link. We therefore call $\mathscr{A}$ the *synchronization* set. Our main result below establishes a practical asymptotic stability result for $\mathscr{A}$, as a function of the coupling gain κ appearing in the flow map (1). The "practical" tuning of κ depends on the following two parameters:

$$\underline{\lambda} := \lambda_{\min}(B^\top B),\ \overline{\omega} := (n-1)|\omega_{\mathrm{M}} - \omega_{\mathrm{m}}| \geq \max_{\widehat{\boldsymbol{\omega}} \in \widehat{\Omega}} |B^\top \widehat{\boldsymbol{\omega}}|_1. \tag{14}$$

Parameter $\underline{\lambda}$ ensures a detectability property of the distance $|x|_{\mathscr{A}}$ in (13) from the norm $|\widehat{\boldsymbol{\sigma}}|$, for any $\widehat{\boldsymbol{\sigma}} \in \widehat{\Sigma}(x)$. In particular, we have from the results in (Godsil and Royle (2001)).

[4] The *tangent cone* to a set $S \subset \mathbb{R}^n$ at a point $x \in \mathbb{R}^n$, denoted $T_S(x)$, is the set of all vectors $w \in \mathbb{R}^n$ for which there exist $x_i \in S$, $\tau_i > 0$ with $x_i \to x$, and $\tau_i \searrow 0$, such that $w = \lim_{i\to\infty} \frac{x_i - x}{\tau_i}$.

Lemma 4. *Since $\mathscr{G}$ is a tree, $\underline{\lambda} := \lambda_{\min}(B^\top B) > 0$.* □

Proof: Consider a tree graph $\mathscr{G}$ with incidence matrix $B \in \mathbb{R}^{n\times n-1}$. By definition $\mathscr{G}$ has only one bipartite connected component. From (Godsil and Royle, 2001, Thm. 8.2.1), $\text{rank}(B) = n-1$ and thus $\dim(\text{null}(B)) = 0$ by way of the fundamental theorem of linear algebra. Therefore, $By \neq 0$ for any $y \in \mathbb{R}^{n-1} \setminus \{\mathbf{0}_{n-1}\}$ which implies $y^\top B^\top B y = |By|^2 > 0$ for any $y \in \mathbb{R}^{n-1} \setminus \{\mathbf{0}_{n-1}\}$. Consequently all the eigenvalues of $B^\top B$ are strictly positive, thus completing the proof. ■

Remark 2. The smallest eigenvalue $\underline{\lambda}$ of $B^\top B$ and its positivity established in Lemma 4 play a fundamental role on the speed of convergence of the closed-loop solutions to the synchronization set. As $\mathscr{G}$ is a tree, positivity of $\underline{\lambda}$ is ensured by Lemma 4. In more general cases with $\mathscr{G}$ not being a tree, the leaderless context considered in this paper, where the synchronized motion emerges from the network, poses significant obstructions to achieving global results. A simple insightful example of a cyclic graph is discussed in Section 5.2, which provides a clear illustration of the motivation behind requiring that $\mathscr{G}$ is a tree. We emphasize that a similar obstruction is experienced in prior work (Mayhew et al. (2012b)) where, in a different context, a similar assumption on the network is required. □

We are now ready to state the main result of this paper, corresponding to a practical $\mathscr{KL}$ bound on the distance of x from $\mathscr{A}$ that is uniform in κ. We state the bound in our main theorem below, whose proof is given in Section 8.2, and then illustrate its relevance on a number of corollaries given next.

Theorem 1. *Given set $\mathscr{A}$ in* (13)*, there exists a class $\mathscr{KL}$ function $\beta_\circ$ and a class $\mathscr{K}$ gain $\gamma_\circ$, both of them independent of κ, such that, for any $\kappa > 0$, all solutions x of* (8) *satisfy*

$$|x(t,j)|_{\mathscr{A}} \leq \beta_\circ(|x(0,0)|_{\mathscr{A}}, \kappa t) + \gamma_\circ((\kappa\underline{\lambda})^{-1} c\overline{\omega}), \tag{15}$$

for all $(t,j) \in \text{dom}\, x$ and with $c := \max_{s\in\text{dom}\,\sigma} \widehat{\sigma}(s)$. □

The bound (15) in Theorem 1 is the sum of two terms: $\beta_\circ$ captures the phases tendency to synchronize, while function $\gamma_\circ$ depends on the mismatch among the (possibly) non-identical, time-varying natural frequencies of the oscillators, which hampers asymptotic phase synchronization in general. Therefore, Theorem 1 provides an insightful bound (15) illustrating the trend of the continuous-time evolution of the hybrid solutions to (8). Notice that $\beta_\circ$ and $\gamma_\circ$ can be constructed by following similar steps as the ones in (Sontag and Wang, 1995, Lemma 2.14), noting that the resulting bound is often subject to some conservatism. On the other hand, because $\beta_\circ$ and $\gamma_\circ$ are independent of κ and $\underline{\lambda}$, (15) still provides valuable quantitative information. Indeed, in view of (15), increasing κ speeds up the transient and reduces the asymptotic phase disagreement caused by the non-identical time-varying natural frequencies. Equation (15) also highlights the impact of the algebraic connectivity $\underline{\lambda}$ of $\mathscr{G}$ (Mesbah and Egerstedt, 2010, pages 23-24) on the phase synchronization, by giving information on the scalability of our algorithm. Recall that $\underline{\lambda}$ is influenced by several parameters of

the undirected graph, such as the maximum degree and the number of nodes (Rad et al. (2011)). This continuous-time focus in (15) in Theorem 1 is motivated by Proposition 1. It is also of interest to establish a bound similar to (15) while measuring the elapsed time in terms of $t+j$ and not only in terms of t, as usually done when defining bounds for solutions to hybrid systems, which allows us to ensure stronger stability properties, in particular, uniformity and robustness (Goebel et al., 2012, Chp.7). Hence, combining Theorem 1 with Proposition 1, we obtain the following second main result.

Theorem 2. *For each value $\kappa > 0$, there exists a class $\mathcal{KL}$ function β such that all solutions to* (8) *satisfy*

$$|x(t,j)|_{\mathcal{A}} \leq \beta(|x(0,0)|_{\mathcal{A}}, t+j) + \gamma_\circ((\kappa\underline{\lambda})^{-1}c\overline{\omega}), \qquad (16)$$

for all $(t,j) \in \operatorname{dom} x$, with $\gamma_\circ$ as in Theorem 1. □

Proof: Let $\kappa > 0$ and x be a solution to (8). In view of Proposition 1, $\frac{1}{\tau_D}t + J_0 \geq j$ for any $(t,j) \in \operatorname{dom} x$, which is equivalent to $\frac{1}{2}t \geq \frac{\tau_D}{2}(j - J_0)$. Hence, we derive from (15), for any $(t,j) \in \operatorname{dom} x$,

$$\begin{aligned}
&\beta_\circ(|x(0,0)|_{\mathcal{A}}, \kappa t) = \beta_\circ\left(|x(0,0)|_{\mathcal{A}}, \kappa(\frac{1}{2}t + \frac{1}{2}t)\right)\\
&\leq \beta_\circ\left(|x(0,0)|_{\mathcal{A}}, \kappa \max\left\{0, \frac{1}{2}t + \frac{\tau_D}{2}j - \frac{\tau_D}{2}J_0\right\}\right)\\
&\leq \beta_\circ\left(|x(0,0)|_{\mathcal{A}}, \frac{\kappa}{2}\max\{0, \min(1,\tau_D)(t+j) - \tau_D J_0\}\right)\\
&=: \beta(|x(0,0)|_{\mathcal{A}}, t+j). \qquad (17)
\end{aligned}$$

Function β is of class $\mathcal{KL}$. Hence, (15) and (17) yield (16), thus completing the proof. ■

Theorem 2 implies that the oscillator phases uniformly converge to any desired neighborhood of $\mathcal{A}$ by taking κ sufficiently large, thus the practical nature of the result. We also immediately conclude from Theorem 2 and Lemma 3 that the stability property in (16) is robust in the sense of item (a) of (Goebel et al., 2012, Def. 7.18), according to (Goebel et al., 2012, Thm. 7.21).

We may draw an important additional conclusion from Theorem 2 corresponding to a global practical $\mathcal{KL}$ bound stemming from the fact that the function $\gamma_\circ$ in (16) is independent of κ.

Corollary 1. *Set $\mathcal{A}$ is uniformly globally practically $\mathcal{KL}$ asymptotically stable for system* (8)*, i.e., for each $\varepsilon > 0$, there exists $\kappa^\star > 0$ such that, for all $\kappa \geq \kappa^\star$, there exists $\beta \in \mathcal{KL}$ such that any solution x verifies $|x(t,j)|_{\mathcal{A}} \leq \beta(|x(0,0)|_{\mathcal{A}}, t+j) + \varepsilon$, for all $(t,j) \in \operatorname{dom} x$.* □

Lastly, in the case of uniform frequencies $\boldsymbol{\omega}(\theta,t) = \mathbf{1}_n\omega(t)$, for all $t \geq 0$, with $\omega(t) \in \Omega$, we have $B^\top\boldsymbol{\omega}(t) = 0$, for all $t \geq 0$. Then, we can exploit the fact that the term $|\overline{\omega}|$ at the right-hand side of (16) stems from upper bounding $|B^\top\widehat{\boldsymbol{\omega}}|_1$ as in (14), which allows obtaining the following asymptotic property of $\mathcal{A}$.

Corollary 2. *If $\boldsymbol{\omega}(\theta,t) = \mathbf{1}_n\omega(t)$, for all $t \geq 0$, with $\omega(t) \in \Omega$, then set $\mathcal{A}$ is uniformly globally $\mathcal{KL}$ asymptotically stable for system* (8)*, i.e., for each $\kappa > 0$, there exists $\beta \in \mathcal{KL}$ such that any solution x verifies*

$$|x(t,j)|_{\mathcal{A}} \leq \beta(|x(0,0)|_{\mathcal{A}}, t+j), \quad \forall (t,j) \in \operatorname{dom} x. \qquad (18)$$

□

5.2. Cyclic graphs and their potential issues

Before proceeding with the technical derivations needed to prove Theorem 1, we devote some attention to the issues pointed out in Remark 2 about the need for the graph $\mathcal{G}$ to be a tree, similar to (Mayhew et al. (2012b)).

Consider system (7) with $n = 3$ and with $\mathcal{G}_u$ an all-to-all undirected graph, thus not a tree. Let $\mathcal{G}$ be the orientation of $\mathcal{G}_u$ with the incidence matrix $B = \left[\begin{smallmatrix} -1 & 0 & 1 \\ 1 & -1 & 0 \\ 0 & 1 & -1 \end{smallmatrix}\right]$. We take $\delta = \frac{3}{4}\pi$, any $\kappa > 0$, any σ satisfying Property 1, and we select for convenience $\boldsymbol{\omega}(\theta,t) = \mathbf{0}_3$ for any time $t \geq 0$ and $x \in X$. Let $x = (\theta, q)$ be a solution to the corresponding system (7) initialized at $\left(-\frac{2}{3}\pi, 0, \frac{2}{3}\pi, 0, 0, 1\right)$. We have that $x(0,0) \in \operatorname{int}(C) \setminus \mathcal{A}$ and $B^\top\theta(0,0) + 2\pi q(0,0) = \frac{2}{3}\pi\mathbf{1}_3$, thus implying $\boldsymbol{\sigma}(x(0,0)) = \sigma(\frac{2}{3}\pi)\mathbf{1}_3$. Hence, because $B\mathbf{1}_3 = 0$, from (2) it holds that $\dot{\theta}(0,0) = \mathbf{0}_3$, and consequently $\operatorname{dom} x \subset [0,\infty) \times \{0\}$, and $x(t,0) = x(0,0)$ and $x(t,0) \in \operatorname{int}(C)\setminus\mathcal{A}$ for all $(t,0) \in \operatorname{dom} x$. As a result, solution x does not converge to the synchronization set.

More generally, when the graph is not a tree, the kernel of matrix B contains additional elements besides the zero vector. Consequently, we can have $B\boldsymbol{\sigma}(x) = \mathbf{0}_n$ even when $x \notin \mathcal{A}$, and $\underline{\lambda} = 0$ in (14). As a result, $\mathcal{A}$ is not globally attractive.

5.3. A Lyapunov-like function and its properties

To prove Theorem 1, we rely on the Lyapunov function V, defined as

$$V(x) := \sum_{(i,j)\in\mathcal{E}} V_{ij}(x), \qquad \forall x \in X, \qquad (19)$$

$$V_{ij}(x) := \int_0^{\theta_j - \theta_i + 2q_{ij}\pi} \sigma(\operatorname{sat}_{\pi+\delta}(s))ds, \qquad (20)$$

with $\operatorname{sat}_{\pi+\delta}(s)$ given by

$$\operatorname{sat}_{\pi+\delta}(s) := \max\left\{\min\{s, \pi+\delta\}, -\pi-\delta\right\}, \quad \forall s \in \mathbb{R}.$$

Function V enjoys useful relations with the distance of x from the synchronization set $\mathcal{A}$, as formalized next.

Lemma 5. *Given function V in* (19)-(20)*, there exist $\alpha_1, \alpha_2 \in \mathcal{K}_\infty$ independent of $\overline{\omega}$ in* (14) *and of κ, such that*

$$\alpha_1(|x|_{\mathcal{A}}) \leq V(x) \leq \alpha_2(|x|_{\mathcal{A}}), \quad \forall x \in X. \qquad (21)$$

□

Proof: For each $x \in \mathscr{A}$, $V(x) = 0$ in view of (13), (19), (20), and for each $x \in (C \cup D) \setminus \mathscr{A}$, $V(x) > 0$ in view of item b) of Property 1. In addition, V is (vacuously) radially unbounded as X is compact. Hence, (21) holds from (Goebel et al., 2012, Page 54). ■

To prove Theorem 1, it is also fundamental to formalize the relation between the distance of x from the set $\mathscr{A}$ and $\widehat{\Sigma}(x)$ in (8), as done in the next lemma.

Lemma 6. *There exists a class $\mathscr{K}_\infty$ function η such that, for each $x \in X$, $\eta(|x|_{\mathscr{A}}) \leq |\widehat{\boldsymbol{\sigma}}|^2, \quad \forall \widehat{\boldsymbol{\sigma}} \in \widehat{\Sigma}(x)$.* □

Proof: From items a) and b) of Property 1, $|\sigma(s)| \geq \alpha(|s|)$ for any $s \in \operatorname{dom}\sigma$. Thus, in view of (9), $|\varsigma| \geq \alpha(|s|)$, for any $s \in \operatorname{dom}\sigma$ and $\varsigma \in \widehat{\sigma}(s)$. We recall that, for any $x \in X$, $\widehat{\Sigma}(x)$ is the stacking of all the set-valued maps $\widehat{\sigma}_{ij}$ defined in (10), $(i,j) \in \mathscr{E}$. Hence, by definition of $\mathscr{A}$, for any $x \in X \setminus \mathscr{A}$, there exists at least one element $\tilde{\theta}_{ij} \neq 0$, with $(i,j) \in \mathscr{E}$, thus $\widehat{\boldsymbol{\sigma}} \in \widehat{\Sigma}(x)$ implies that $|\widehat{\boldsymbol{\sigma}}| \geq |\widehat{\sigma}_{ij}(x)| \geq \alpha(|\tilde{\theta}_{ij}|)$. Similarly, for any $x \in \mathscr{A}$, $|\widehat{\boldsymbol{\sigma}}| \geq |\widehat{\sigma}_{ij}(x)| \geq \alpha(|\tilde{\theta}_{ij}|) = 0$. Therefore, $\max_{(i,j)\in\mathscr{E}} \alpha(|\tilde{\theta}_{ij}|)$ is a suitable lower bound for $|\widehat{\boldsymbol{\sigma}}|$, for any $x \in X$. Since $\tilde{\theta}_{ij}$ is a function of the states and $\max_{(i,j)\in\mathscr{E}} \alpha(\cdot)$ is positive definite and radially unbounded, as X is compact, then (Goebel et al., 2012, Page 54) implies that there exists $\eta \in \mathscr{K}_\infty$ such that $\eta(|x|_{\mathscr{A}}) \leq |\widehat{\boldsymbol{\sigma}}|^2$ holds for each $x \in X$ and for all $\widehat{\boldsymbol{\sigma}} \in \widehat{\Sigma}(x)$, thus concluding the proof. ■

Function V is locally Lipschitz due to the properties of σ and characterizing its variation when evaluated along the solutions of the hybrid inclusion (8) requires using tools from non-smooth analysis. To avoid breaking the flow of the exposition, we postpone to Section 8.2 those technical derivations and summarize the corresponding conclusions in the next proposition, a key result for proving Theorem 1.

Proposition 2. *Consider system* (8) *and function V in* (19)-(20). *There exist $\alpha_3 \in \mathscr{K}_\infty$ independent of $\overline{\omega}$ in* (14) *and of κ, such that for any $\kappa > 0$, any solution x of* (8) *satisfies (denoting $\operatorname{dom} x = \bigcup_{j=0}^{J} [t_j, t_{j+1}] \times \{j\}$, possibly with $J = +\infty$) (i) for all $j \in \{0, \dots, J\}$ and almost all $t \in [t_j, t_{j+1}]$,*

$$\frac{d}{dt} V(x(t,j)) \leq -\kappa \underline{\lambda} \alpha_3(V(x(t,j))) + c\overline{\omega}, \tag{22a}$$

with c defined in Theorem 1;
(ii) for all $j \in \{0, \dots, J-1\}$,

$$V(x(t, j+1)) \leq V(x(t,j)). \tag{22b}$$

□

We are now ready to present the proof of Theorem 1.

Proof of Theorem 1: Let $\kappa > 0$ and x be a solution (8) and denote, with a slight abuse of notation, $\operatorname{dom} x = \bigcup_{j=0}^{J} [t_j, t_{j+1}] \times \{j\}$ with $J \in \mathbb{Z}_{\geq 0} \cup \{+\infty\}$. We scale the continuous time as $\tau := (\kappa\underline{\lambda})t \in \mathbb{R}_{\geq 0}$ and we denote $\tau_j := (\kappa\underline{\lambda})t_j$ and $V'(x(\cdot,\cdot))$ the time-derivative of V with respect to τ. From item (i) of Proposition 2, for all $j \in \{0, \dots, J\}$ and almost all $\tau \in [\tau_j, \tau_{j+1}]$,

$$\begin{aligned} V'(x(\tau, j)) &= (\kappa\underline{\lambda})^{-1} \dot{V}(x(t,j)) \\ &\leq -\alpha_3(V(x(t,j))) + (\kappa\underline{\lambda})^{-1} c\overline{\omega}. \end{aligned} \tag{23}$$

Combining (23) with the non-increase condition in (22b), we follow the steps of the proof of (Sontag and Wang, 1995, Lemma 2.14) to obtain an input-to-state stability bound on $V(\tilde{x}(\cdot,\cdot))$ where $\tilde{x}(\cdot,\cdot) := x((\kappa\underline{\lambda})^{-1}(\cdot),(\cdot)) = x(\cdot,\cdot)$, which can then be converted to a bound on $|x(\cdot,\cdot)|_{\mathscr{A}}$ using (21), thus leading to (15), where $\beta_\circ$ and $\gamma_\circ$ only depend on α_1, α_2 and α_3 and are therefore independent of $\overline{\omega}$ and κ. Note that the dependence on $\underline{\lambda}$ is left implicit in $\beta_\circ$ and $\gamma_\circ$. ■

6. Prescribed finite-time stability properties

A useful outcome of the mild regularity conditions that we require from σ in Property 1 is that defining σ to be discontinuous at the origin, as in the sign function represented in Figure 1, leads to desirable sliding-like behavior of the solutions in the attractor $\mathscr{A}$. This sliding property induces interesting advantages of the behavior of solutions, as compared to the general asymptotic and practical properties characterized in Section 5.

A first advantage is that, even with non-uniform natural frequencies, we prove uniform global $\mathscr{KL}$ asymptotic stability of $\mathscr{A}$ for a large enough coupling gain κ, due to the well-known ability of sliding-mode mechanisms to dominate unknown additive bounded disturbances acting on the dynamics. A second advantage is that the Lyapunov decrease characterized in Proposition 2 can be associated with a guaranteed constant negative upper bound outside $\mathscr{A}$, which implies finite-time convergence. Finally, since this constant upper bound can be made arbitrarily negative by taking κ sufficiently large, we actually prove prescribed finite-time convergence (see (Song et al. (2017))) when using these special discontinuous functions σ, whose peculiar features are characterized in the next lemma.

Lemma 7. *Given a function σ satisfying Property 1, if σ is discontinuous at the origin, then there exists $\mu > 0$ such that, for any $x \in X \setminus \mathscr{A}$, $|\widehat{\boldsymbol{\sigma}}| \geq \mu$, for all $\widehat{\boldsymbol{\sigma}} \in \widehat{\Sigma}(x)$.* □

Proof: Since σ is discontinuous at 0 and it is piecewise continuous, there exists $\varepsilon > 0$ such that σ is continuous in $[-\varepsilon, 0)$ and $(0, \varepsilon]$. By item a) of Property 1, $\lim_{s\to 0^+} \sigma(s) = -\lim_{s\to 0^-} \sigma(s) =: \sigma_\circ \neq 0$ as σ is discontinuous at 0 and $\sigma(0) = 0$. Then there exists $\varepsilon_\circ \in (0, \varepsilon]$ such that $\sigma(s) \geq \frac{\sigma_\circ}{2}$ for all $s \in (0, \varepsilon_\circ]$. From item b) of Property 1, for any $s \in [\varepsilon_\circ, \pi + \delta]$, $\sigma(s) \geq \alpha(\varepsilon_\circ) > 0$. Hence, due to item a) of Property 1, $|\sigma(s)| \geq \mu := \min(\frac{\sigma_\circ}{2}, \alpha(\varepsilon_\circ))$ for all $s \in \operatorname{dom}\sigma \setminus \{0\}$. Moreover, in view of (9), for any $s \in \operatorname{dom}\sigma \setminus \{0\}$ and any $\varsigma \in \widehat{\sigma}(s)$, $|\varsigma| \geq \mu$. Since, for any $x \in X$, $\widehat{\Sigma}(x)$ is the stacking of all the set-valued maps $\widehat{\sigma}_{ij} = \widehat{\sigma}$, $(i,j) \in \mathscr{E}$, and by definition of $\mathscr{A}$,

for any $x \in X \setminus \mathscr{A}$, there exists at least one nonzero element $\tilde{\theta}_{ij} \neq 0$ for some $(i,j) \in \mathscr{E}$. Then $\widehat{\boldsymbol{\sigma}} \in \widehat{\Sigma}(x)$ implies $|\widehat{\boldsymbol{\sigma}}| \geq |\widehat{\sigma}_{ij}(x)| \geq \mu$, thus concluding the proof. ■

Paralleling the structure of Proposition 2, the next proposition, whose proof is postponed to Section 8.3, is a key result for proving Theorem 3.

Proposition 3. *Consider system* (8) *and function* V *in* (19)-(20). *If* σ *is discontinuous at the origin, then there exist* $\mu \in \mathbb{R}_{>0}$ *independent of* $\overline{\omega}$ *in* (14) *and* $\kappa^\star > 0$ *such that for each* $\kappa \geq \kappa^\star$ *any solution* x *of* (8) *satisfies (denoting* $\operatorname{dom} x = \bigcup_{j=0}^{J} [t_j, t_{j+1}] \times \{j\}$, *possibly with* $J = +\infty$*)*
(i) for all $j \in \{0, \dots, J\}$ *and almost all* $t \in [t_j, t_{j+1}]$ *such that* $x(t,j) \notin \mathscr{A}$,

$$\frac{d}{dt} V(x(t,j)) \leq -\frac{1}{2}\kappa \underline{\lambda} \mu^2; \tag{24a}$$

(ii) for all $j \in \{0, \dots, J-1\}$,

$$V(x(t,j+1)) \leq V(x(t,j)). \tag{24b}$$

□

Exploiting Lemma 7 and Proposition 3, we can follow similar steps to those in the proof of Theorem 1 to show the following main result on uniform global $\mathscr{KL}$ asymptotic stability and prescribed finite-time stability of $\mathscr{A}$ for (8).

Theorem 3. *If* σ *is discontinuous at the origin, then set* $\mathscr{A}$ *in* (13) *is prescribed finite-flowing-time stable for* (8), *i.e., for each* $T > 0$ *there exists* $\kappa^\star > 0$ *such that for each* $\kappa \geq \kappa^\star$*:*
(i) there exists $\beta \in \mathscr{KL}$ *such that all solutions* x *satisfy* (18)*;*
(ii) all solutions x *satisfy,* $x(t,j) \in \mathscr{A}$ *for all* $(t,j) \in \operatorname{dom} x$ *with* $t \geq T$. □

Proof: We start showing that $G(D \cap \mathscr{A}) \subset \mathscr{A}$. Indeed, we notice that $D_{ij} \cap \mathscr{A} = \emptyset$ for any $(i,j) \in \mathscr{E}$, and thus $G(D_{ij} \cap \mathscr{A}) \subset \mathscr{A}$ trivially holds. Moreover, from Lemma 2, it holds that $G(D_i \cap \mathscr{A}) \subset \mathscr{A}$ for any $i \in \mathscr{V}$. Hence, from (7b), we conclude that $G(D \cap \mathscr{A}) \subset \mathscr{A}$. To establish that $\mathscr{A}$ is (strongly) forward invariant for (8), it is left to prove that solutions cannot leave $\mathscr{A}$ while flowing. We proceed by contradiction and for this purpose suppose there exists a solution x_{bad} to (8) such that $x_{\text{bad}}(0,0) \in \mathscr{A}$ and $x_{\text{bad}}(t^*,0) \notin \mathscr{A}$ for some $t^* > 0$ with $(t^*,0) \in \operatorname{dom} x_{\text{bad}}$. From continuity of flowing solutions between any two successive jumps and closedness of $\mathscr{A}$, there exists $x_{\text{bad}}(t,0) \in \mathscr{A}$ for all $t \in [0,t^*)$ and $x_{\text{bad}}(t^*,0) \notin \mathscr{A}$. Hence, from (19) and (20) and positive definiteness of V, we have $0 = V(x_{\text{bad}}(0,0)) < V(x_{\text{bad}}(t^*,0))$. However, since the solution is flowing, integrating (24a) over the continuous time interval $[0,t^*]$ we obtain $V(x_{\text{bad}}(t^*,0)) < V(x_{\text{bad}}(0,0))$, which establishes a contradiction. Consequently, a solution cannot leave $\mathscr{A}$ while flowing. We have proven that the set $\mathscr{A}$ is (strongly) forward invariant, implying that if $x(t,j) \in X \setminus \mathscr{A}$ then $x(t',j') \in X \setminus \mathscr{A}$, for any $t' + j' \leq t + j$, with $(t',j'),(t,j) \in \operatorname{dom} x$. Let $\kappa \geq \kappa^\star$ with $\kappa^\star$ defined in Proposition 3 and x be a solution to (8). Combining (24a) with the non-increase condition (24b) and the forward invariance of $\mathscr{A}$, we obtain by integration for any $(t,j) \in \operatorname{dom} x$

$$V(x(t,j)) \leq -\frac{1}{2}\kappa \underline{\lambda} \mu^2 t + V(x(0,0)), \tag{25}$$

whenever $x(t,j) \in X \setminus \mathscr{A}$, and thus

$$V(x(t,j)) \leq \max(-\frac{1}{2}\kappa \underline{\lambda} \mu^2 t + V(x(0,0)), 0), \tag{26}$$

for any $x(t,j) \in X$. Equation (26) can then be converted to a bound on $|x(t,j)|_{\mathscr{A}}$ using (21). Hence, we follow the same steps used in the proofs of Theorem 1 and 2 to obtain (18), thus concluding the proof of item (i) in Theorem 3. In view of (25) and from the positive definiteness of V with respect to $\mathscr{A}$, we conclude that solutions to (8) reach the synchronization set $\mathscr{A}$ flowing at most for $T := \frac{1}{\kappa}\frac{2\overline{v}}{\underline{\lambda}\mu^2}$, where $\overline{v} := \max_{x \in X} V(x)$. Hence, in view of the forward invariance of $\mathscr{A}$, item (ii) in Theorem 3 holds thus completing the proof. ■

Notice that phases synchronize at most at continuous time $T = \frac{1}{\kappa}\frac{2\overline{v}}{\underline{\lambda}\mu^2}$, in view of (26). Therefore, we may decrease T at will by selecting a larger μ as in Lemma 7 and/or by increasing the coupling gain κ.

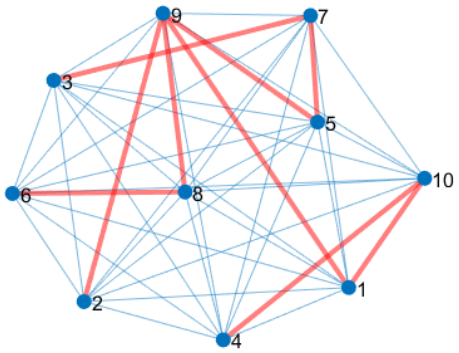

Figure 3: The networks of oscillators described in Section 7: the blue graph depicts physical couplings captured by ω_i in (27), and the red graph is the communication tree graph that we design for the hybrid coupling rules presented in Section 3.

7. Numerical illustration

In this section, we apply our control scheme to globally, uniformly, synchronize the phases of $n = 10$ strongly damped generators physically coupled over an all-to-all network connection (represented by the blue edges in Figure 3) over a set $\mathscr{V}$ of nodes whose dynamics are approximated by nonuniform first-order Kuramoto oscillators given by (Dörfler and Bullo, 2012, eq. (2.8)). This fully connected dynamics can be accurately described by the terms ω_i's in (1) with the following selection:

$$\omega_i(\theta,t) := \frac{1}{\zeta_i}\Big(\widetilde{\omega}_i\Big(1 + \frac{3}{10}\sin(\chi_i t + \phi_i)\Big) + d_i(t) - \widetilde{\kappa}_{ij} \sum_{j \in \mathscr{V}\setminus\{i\}} \sin(\theta_j - \theta_i + \phi_{ij})\Big), \ \forall i \in \mathscr{V}, \tag{27}$$

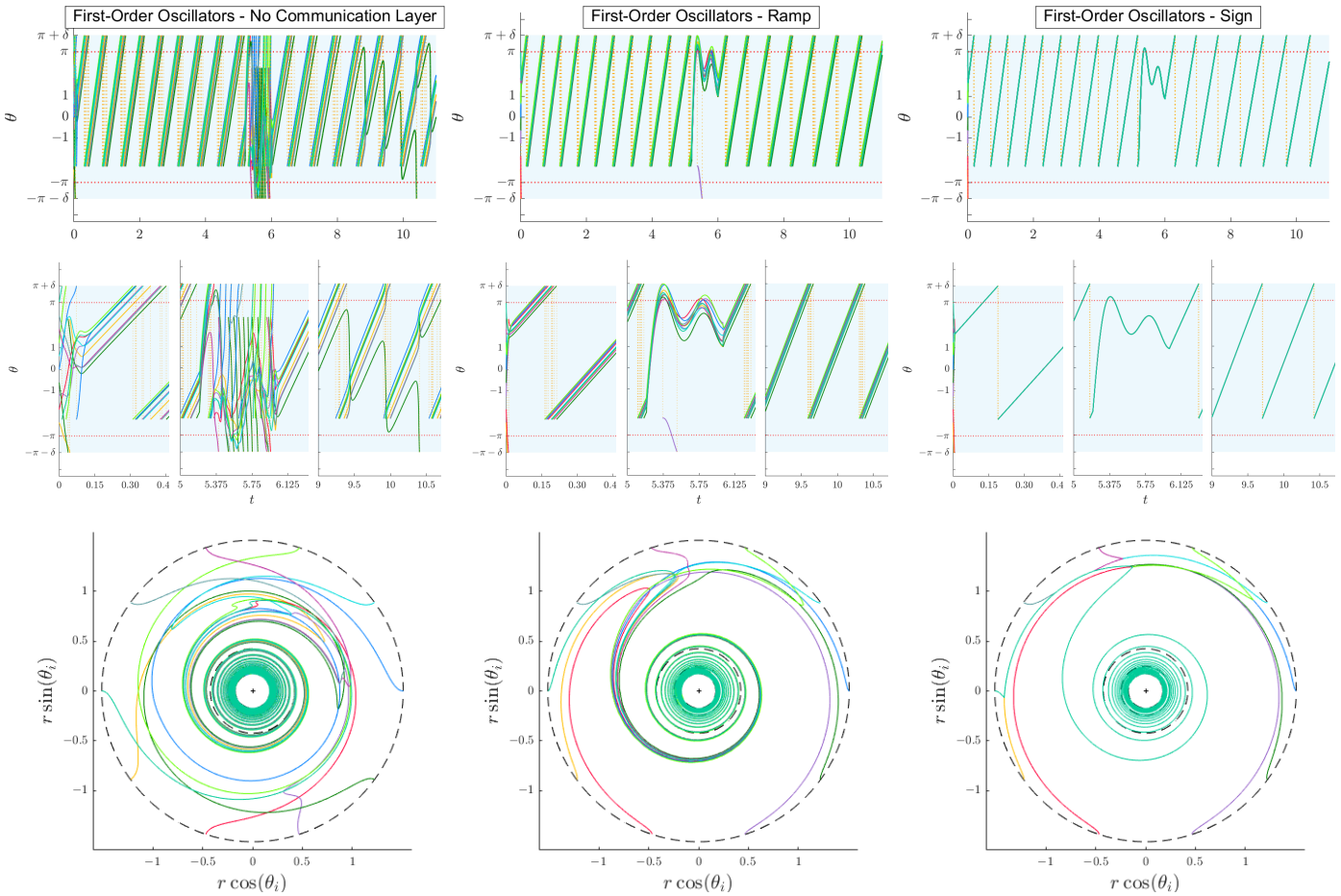

Figure 4: (Top) Phase evolution for $\kappa = \frac{576\pi}{10}$, $\delta = \frac{\pi}{4}$ and different selections of σ and communication configurations. (Middle) Phase evolution in the time intervals $[0, 0.41]$, $[5, 5.2]$ and $[9, 10.75]$. (Bottom) Evolution of the pair $(r\cos(\theta_i), r\sin(\theta_i))$, with $r(t) = (1.55\sqrt{t} + 0.66)^{-1}$, showing radially the continuous-time evolution for the phases generated by our hybrid modification (7). The black dashed lines are isotime (0 (outer), 3.66, 7.33 and 11 (inner) time units).

for generic constant parameters $\chi_i \in \text{uni}([-1,1])$, $\widetilde{\omega}_i \in \text{uni}([-5,5])$, $\phi_i \in \text{uni}([0, \text{atan}(0.25)])$, and $\zeta_i \in \text{uni}([20,30]\frac{1}{120\pi})$. The physical all-to-all coupling among the oscillators (blue edges in Figure 3) is modeled by the sine functions $\sin(\theta_j - \theta_i + \phi_{ij})$ of the angular mismatch between the oscillators offsetted by the constant angle $\phi_{ij} \in \text{uni}([0, \text{atan}(0.25)])$. Furthermore, each physical coupling is scaled by the gain $\widetilde{\kappa}_{ij} = \widetilde{\kappa}_{ji} \in \text{uni}([0.7, 1.2])$. This allows fully embedding in our time-varying generalized natural frequencies ω_i of (1) the physical couplings of the oscillators. Each high-frequency disturbance $d_i : \mathbb{R}_{\geq 0} \to [0,5]$ is defined as $d_i(s) = 0$ if $s \in [0, 5.2] \cup [6.0, 11]$ and $d_i(s) = 5\sin(50\chi_i s + \phi_i)$ if $s \in (5.2, 6)$. Thus $\omega_i(\theta, t)$ not only captures the time-varying natural frequency of the i-th oscillator but also the physical coupling actions and disturbances influencing its dynamics. The parameters have been selected as in (Dörfler and Bullo (2012)) to model realistic, strongly damped, generators. On the other hand, the synchronizing coupling actions are exchanged through our communication graph $\mathcal{G}_u = (\mathcal{V}, \mathcal{E}_u)$, whose edges are depicted in red in Figure 3. These "cyber" coupling actions are represented by the functions σ's in (1), whose design is performed according to our solution of Section 3. Summarizing, the combination of the (blue) physical layer and the (red) "cyber" communication layer of Figure 3 generates a cyber-physical system whose dynamics is represented by (2), (7), with $\boldsymbol{\omega}$ capturing the physical layer and $\boldsymbol{\sigma}$ capturing the hybrid feedback control action. We initialize the oscillators with $q(0,0) = \mathbf{0}_9$ and the initial phases are chosen in such a way that the oscillators are equally spaced on the unit circle. Finally, we select $\delta = \frac{\pi}{4}$.

The evolution of the phases, $\theta_i's$, and the angular errors between any two neighbours in $\mathcal{G}$, namely $\min_{h\in\{-1,0,1\}}(|\theta_j - \theta_i + 2h\pi|)$, are reported[5] in the top two rows of Figure 4 and in Figure 5, for different selections of σ, and $\kappa = \frac{576\pi}{10}$, which ensure finite-time synchronization due to the bound reported in Lemma 10 in Section 8.3. When no communication layer is considered (left plots), the oscillators do not synchronize. When the communication layer is implemented and σ is given as the ramp function, practical synchronization is achieved as established in Theorem 1 and shown in

[5]The simulations have been carried out using the Matlab toolbox HyEQ (Sanfelice et al. (2013)).

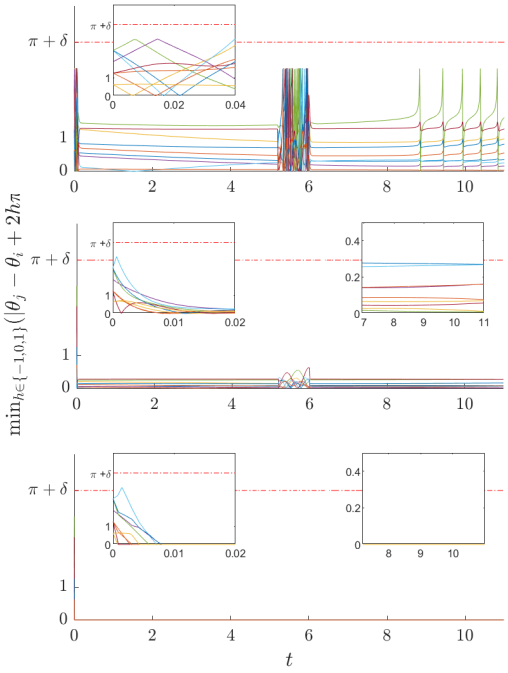

Figure 5: Evolution of the phase errors for $\kappa = \frac{576\pi}{10}$ and different selections of σ and communication configurations (from top to bottom: no communication layer, ramp and sign functions).

Figures 4 and 5. (Non-uniform) practical synchronization can also be achieved in the absence of a communication layer by selecting larger values for the $\widetilde{\kappa}_{ij}$'s. On the other hand, the sign function, which is discontinuous at 0, also leads to a finite-time synchronization property in agreement with Theorem 3, see Figures 4 and 5. Furthermore, the set of plots in the bottom row of Figure 4 shows that each phase θ_i maps continuously the angular values identifying oscillator i on the unit circle, in agreement with Section 3.1 and Lemma 2.

The same exact hybrid controller dynamics is finally exploited in a more sophisticated context of non-strongly damped generators (rather than the strongly damped case, as considered above and in Figures 4 and 5). Following (Dörfler and Bullo (2012)), such behavior is modeled by a fully connected graph comprising the second-order (rather than first-order) heterogeneous oscillators in (Dörfler and Bullo, 2012, eq. (2.3)). Once again, this physical interconnection is well represented by the blue edges in Figure 3 and dynamics (1) with the following selection, generalizing (27) to the dynamical context,

$$\dot{\omega}_i(\theta,\mathrm{t}) = -\frac{\zeta_i}{m_i}\omega_i(\theta,\mathrm{t}) + \frac{1}{m_i}\Bigg(\widetilde{\omega}_i\Big(1+\frac{3}{10}\sin(\chi_i\mathrm{t}+\phi_i)\Big) + d_i(\mathrm{t}) - \widetilde{\kappa}_{ij}\sum_{j\in\mathcal{V}\setminus\{i\}}\sin(\theta_j-\theta_i+\phi_{ij})\Bigg),\ \forall i\in\mathcal{V}. \tag{28}$$

This dynamically generalized selection uses the same parameters as in the previous set of simulations, with the addition of the constant mass parameters $m_i \in \mathrm{uni}([2,12]\frac{1}{120\pi})$ for each $i\in\mathcal{V}$, which is defined according to (Dörfler and Bullo, 2012, eq. 2.3). We apply our hybrid feedback control algorithm to this generalized scenario by augmenting once again the physical layer with a "cyber" communication layer represented by the red edges in Figure 3, inducing the stabilizing action of inputs $\boldsymbol{\sigma}$ in the hybrid interconnection (2), (7). We initialize q and θ as in the previous simulations and $\dot{\theta}_i(0,0)\in\mathrm{uni}([-0.1,0.1])$ for each $i\in\mathcal{V}$. Finally, we still select $\delta=\frac{\pi}{4}$ in (3). The evolution of the phases is reported in Figure 6, for different selections of σ, and $\kappa=\frac{576\pi}{10}$. Similarly to what happens for the first-order oscillators of Figures 4 and 5, when no communication layer is considered, the second-order oscillators do not synchronize. When the generators are equipped with the communication network and σ is instead defined as the ramp function, practical synchronization is achieved, as predicted by Theorem 1 and as shown in Figure 6. On the other hand, considering the (discontinuous at 0) sign function to generate the synchronizing hybrid coupling actions again leads to a finite-time synchronization property, thus confirming Theorem 3.

8. Proof of Propositions 2 and 3

8.1. Results on scalar non-pathological functions

The proofs of Propositions 2 and 3, which are instrumental for proving our main results of Sections 5 and 6, require exploiting results from non-smooth analysis, because V in (19) is not differentiable everywhere. A further complication emerges from the fact that, since σ may be discontinuous, the flow map in dynamics (8) is outer semicontinuous, but not inner semicontinuous. The lack of inner semicontinuity prevents us from exploiting the "almost everywhere" conditions of (Della Rossa et al. (2021)) and references therein. Instead, one could resort to conditions involving Clarke's generalized directional derivative and Clarke's generalized gradient, which can be defined as (see (Clarke, 1990, page 11))

$$\partial V(x) := \mathrm{co}\{\lim_{i\to\infty}\nabla V(x_i) : x_i\to x,\ x_i\notin\mathscr{Z},\ x_i\notin\Omega_u\}, \tag{29}$$

where Ω_u is the set (of Lebesgue measure zero) where V is not differentiable, and $\mathscr{Z}$ is any other set of Lebesgue measure zero. However, due to the peculiar dynamics considered here (resembling, for example, the undesirable conservativeness highlighted in (Della Rossa, 2020, Ex. 2.2)), Lyapunov decrease conditions based on Clarke's generalized gradient would be too conservative and impossible to prove. Due to the above motivation, in this section we prove Propositions 2 and 3 by exploiting the results of (Valadier (1989); Bacciotti and Ceragioli (2003)), whose proof is also reported in (Della Rossa, 2020, Lemma 2.23), establishing a link between the time derivative $\frac{d}{dt}V(\phi(\mathrm{t}))$ of a Lyapunov-like function V evaluated along a generic solution ϕ of a continuous-time system, and the so-called set-valued Lie derivative (Bacciotti and Ceragioli (1999))

$$\dot{\overline{V}}_F(x) := \{a\in\mathbb{R}\,|\,\exists f\in F(x) : \langle v,f\rangle = a,\ \forall v\in\partial V(x)\}, \tag{30}$$

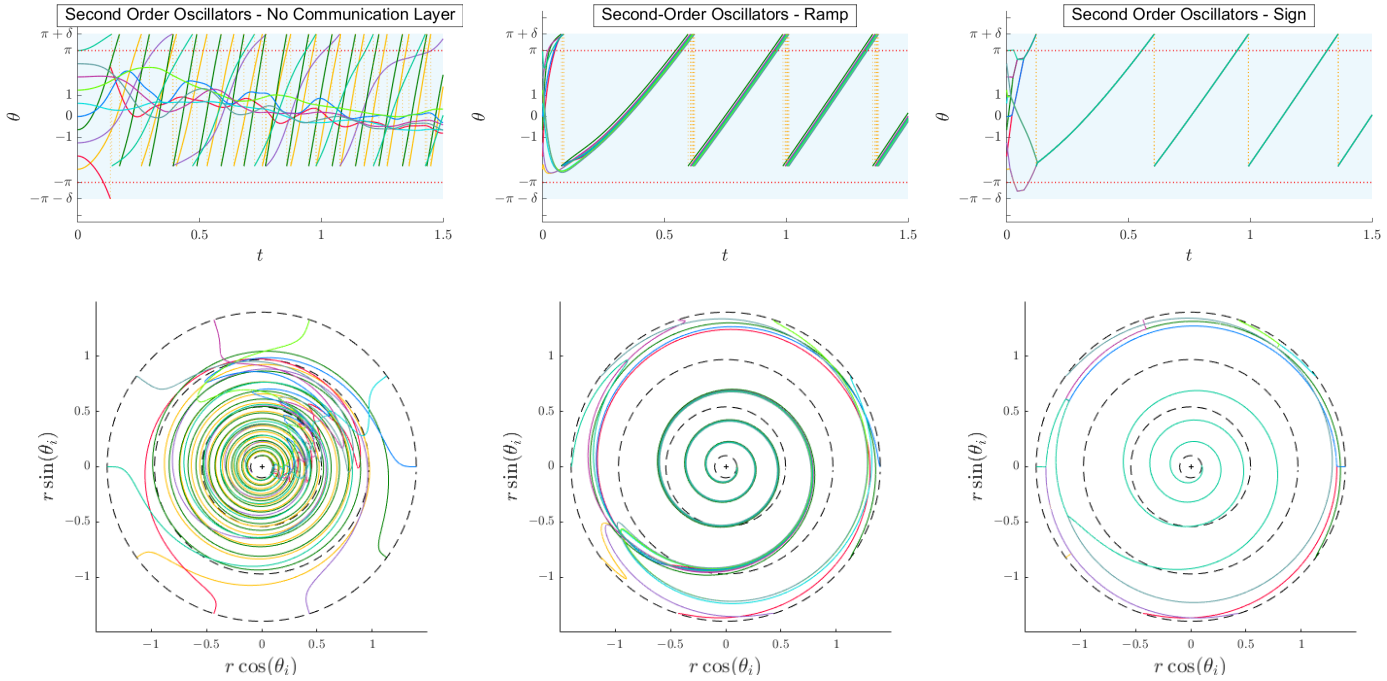

Figure 6: (Top) Phase evolution associated of second-order oscillators for $\kappa = \frac{576\pi}{10}$, $\delta = \frac{\pi}{4}$ and different selections of σ and communication configurations. (Bottom) Evolution of the pair $(r\cos(\theta_i), r\sin(\theta_i))$, with $r(t) = -0.255\sqrt{t} + 1.4$, showing radially the continuous-time evolution for the phases generated by our hybrid modification of second-order oscillators. The black dashed lines are isotime (0 (outer), 0.5, 1 and 1.5 (inner) time units).

with ∂V defined in (29). In the following, we characterize some features of the set-valued Lie derivative, useful for the next technical derivations.

Lemma 8. *Consider a set $S \subset \mathbb{R}^n$, $F : \mathrm{dom}\, F \subset \mathbb{R}^n \rightrightarrows \mathbb{R}^n$ with $S \subset \mathrm{dom}(F)$ and a locally Lipschitz $V : \mathrm{dom}\, V \subseteq \mathbb{R}^n \to \mathbb{R}$ such that $S \subset \mathrm{dom}(V)$. Given any function $\varphi : \mathbb{R}^n \times \mathbb{R}^n \to \mathbb{R}^n$ satisfying $\varphi(x, f) \in \partial V(x)$, $\forall x \in S$, $\forall f \in F(x)$, it holds that*

$$\sup \dot{\overline{V}}_F(x) \leq \sup_{f \in F(x)} \langle \varphi(x, f), f \rangle. \tag{31}$$

□

Proof: Consider any $x \in S$. In view of (30), and by the fact that $\varphi(x, f) \in \partial V(x)$ for all $f \in F(x)$, we have that $a = \langle v, f(x) \rangle \in \dot{\overline{V}}_F(x)$ implies $a = \langle \varphi(x, f), f \rangle$. Hence, we derive that $\dot{\overline{V}}_F(x) \subseteq \bigcup_{f \in F(x)} \{\langle \varphi(x, f), f \rangle\}$ and thus $\sup \dot{\overline{V}}_F(x) \leq \sup_{f \in F(x)} \langle \varphi(x, f), f \rangle$ as to be proven. ■

Whenever function V is non-pathological (according to the definition given next), (Della Rossa, 2020, Lemma 2.23) ensures that $\frac{d}{dt} V(\phi(t)) \in \dot{\overline{V}}_F(\phi(t))$ for almost all t in the domain of ϕ. We provide below the definition of non-pathological functions and we prove that function V in (19) enjoys that property. Our result below can be seen as a corollary of the fact that piecewise C^1 functions (in the sense of (Scholtes (2012))) are non-pathological. This result has been recently published in (Della Rossa et al., 2022, Lemma 4). The scalar case is a consequence of Proposition 5 in (Valadier (1989)). An alternative proof is reported here.

Definition 1. *(Valadier (1989)) A locally Lipschitz function $W : \mathrm{dom}\, W \subseteq \mathbb{R} \to \mathbb{R}$ is* non-pathological *if, given any absolutely continuous function $\phi : \mathbb{R}_{\geq 0} \to \mathrm{dom}\, W$, we have that for almost every $t \in \mathbb{R}_{\geq 0}$ there exists $a_t \in \mathbb{R}$ satisfying*

$$\langle w, \dot{\phi}(t) \rangle = a_t, \quad \forall w \in \partial W(\phi(t)). \tag{32}$$

In other words, for almost every $t \in \mathbb{R}_{\geq 0}$, $\partial W(\phi(t))$ is a subset of an affine subspace orthogonal to $\dot{\phi}(t)$. □

Proposition 4. *Any function $W : \mathrm{dom}\, W \subseteq \mathbb{R} \to \mathbb{R}$ that is piecewise continuously differentiable is non-pathological.* □

For this paper, the interest of Proposition 4 stands in the fact that it implies that function V in (19) is non-pathological (Valadier (1989); Bacciotti and Ceragioli (1999)), being the sum of piecewise continuously differentiable scalar functions.

Remark 3. An alternative proof of Proposition 4, might be to first establish that piecewise C^1 functions from $\mathbb{R} \to \mathbb{R}$ can be represented as a max-min of C^1 functions from $\mathbb{R} \to \mathbb{R}$ (a similar result has been proven, for example, in (Xu et al., 2017, Thm. 1 and Prop. 1) with reference to piecewise affine functions), and then obtain Proposition 4 as a corollary of (Della Rossa, 2020; Valadier, 1989; Bacciotti and Ceragioli, 1999, Lemma 2.20), which establish non-pathological properties of max-min functions. □

Proof of Proposition 4: Let $W : \mathrm{dom}\, W \subseteq \mathbb{R} \to \mathbb{R}$ be piecewise continuously differentiable. Let $\phi : \mathbb{R}_{\geq 0} \to \mathrm{dom}\, W$ be an absolutely continuous scalar function and suppose it is differentiable at $\bar{t} \in \mathbb{R}_{\geq 0}$. We split the analysis in three cases.

a) $\dot{\phi}(\bar{t}) = 0$. Then, for all $w \in \partial W(\phi(\bar{t}))$, $\langle w, \dot{\phi}(\bar{t})\rangle = \langle w, 0\rangle = 0$. Thus, (32) is satisfied with $a_t = 0$.

b) $\dot{\phi}(\bar{t}) > 0$. If W is continuously differentiable at $\phi(\bar{t})$ then, $\partial W(\phi(\bar{t})) = \nabla W(\phi(\bar{t}))$ and (32) holds. Consider now the case where W is not differentiable at $\bar{t}$. We recall that, in view of the fact that W is piecewise continuously differentiable, $\partial W(\phi(t)) = \nabla W(\phi(t))$ for any t in a sufficiently small neighbourhood of $\bar{t}$. From the absolute continuity of ϕ, there exists $\varepsilon > 0$ such that $\lim_{h\to 0} \frac{\phi(\bar{t}+h)-\phi(\bar{t})}{h} \geq \varepsilon > 0$. Hence, there exists $\rho_1 \in \mathbb{R}_{>0}$ such that for any $\rho \in (0, \rho_1]$, we have $\frac{\phi(\bar{t}+\rho)-\phi(\bar{t})}{\rho} \geq \frac{\varepsilon}{2}$ and thus $\phi(\bar{t}+\rho) \geq \frac{\rho\varepsilon}{2} + \phi(\bar{t}) > \phi(\bar{t})$. With a similar reasoning, there exist $\rho_2 \in \mathbb{R}_{\geq 0}$ such that $\rho_2 > 0$ implies $\phi(\bar{t}-\rho) < \phi(\bar{t})$ for any $\rho \in (0, \rho_2]$. Hence, there exists a neighbourhood of $\bar{t}$ contained in $[\bar{t}-\rho_2, \bar{t}+\rho_1]$, for which $\partial W(\phi(\cdot))$ is defined and coincides with $\nabla W(\phi(t))$. Therefore, for almost every $\tilde{t} \in \mathcal{T} \subseteq [\bar{t}-\rho_2, \bar{t}+\rho_1]$ there exists $a_t \in \mathbb{R}$ such that (32) is satisfied.

c) $\dot{\phi}(\bar{t}) < 0$. This case is identical to the previous one by changing all the signs, therefore implying that for almost every t there exists $a_t \in \mathbb{R}$ in a compact neighbourhood of $\bar{t}$ such that (32) is satisfied.

Since ϕ is absolutely continuous, then the set Φ where it is not differentiable is of Lebesgue measure zero. We conclude that (32) is satisfied for almost all $t \in \mathbb{R}_{\geq 0}$ because we have arbitrarily selected $\bar{t} \in \mathbb{R}_{\geq 0} \setminus \Phi$, as to be proven. ■

8.2. Proof of Proposition 2

The following lemma establishes geometric properties of V that are used, together with Lemma 5 and Proposition 4, to show the trajectory-based results of Proposition 2.

Lemma 9. *Consider system* (8)*, function V in* (19)-(20) *and c as in Theorem 1. There exists $\alpha_3 \in \mathcal{K}_\infty$, independent of $\overline{\omega}$ in* (14) *and of κ, such that*

$$\sup \dot{\overline{V}}_F(x) \leq -\kappa \underline{\lambda} \alpha_3(V(x)) + c\overline{\omega}, \qquad \forall x \in C, \tag{33a}$$

$$\Delta V(x) := \sup_{g \in G(x)} V(g) - V(x) \leq 0, \qquad \forall x \in D. \tag{33b}$$

□

Proof: We prove the two equations one by one.

Proof of (33a). For each $x \in C$ and each $f \in F(x)$, there exist $\widehat{\boldsymbol{\omega}} \in \widehat{\Omega}$ and $\boldsymbol{\sigma}_f \in \widehat{\Sigma}(x)$ such that $f = (\widehat{\boldsymbol{\omega}} - B\kappa\boldsymbol{\sigma}_f, 0) \in F(x)$. Define $\varphi(x, f)$ in Lemma 8 as $\varphi(x, f) := (B\boldsymbol{\sigma}_f, 2\pi\boldsymbol{\sigma}_f)$. From (30) in Lemma 8, we have

$$\sup \dot{\overline{V}}_F(x) \leq \sup_{\substack{\widehat{\boldsymbol{\omega}} \in \widehat{\Omega}, \\ \boldsymbol{\sigma}_f \in \widehat{\Sigma}(x)}} (-\kappa \boldsymbol{\sigma}_f^\top B^\top B \boldsymbol{\sigma}_f + \boldsymbol{\sigma}_f^\top B^\top \widehat{\boldsymbol{\omega}}). \tag{34}$$

Thus, in view of (14) and Lemma 4, (34) yields

$$\begin{aligned} \sup \dot{\overline{V}}_F(x) &\leq \sup_{\boldsymbol{\sigma}_f \in \widehat{\Sigma}(x)} (-\kappa \boldsymbol{\sigma}_f^\top B^\top B \boldsymbol{\sigma}_f) + c\overline{\omega} \\ &\leq \sup_{\boldsymbol{\sigma}_f \in \widehat{\Sigma}(x)} -\kappa \underline{\lambda} |\boldsymbol{\sigma}_f|^2 + c\overline{\omega}. \end{aligned} \tag{35}$$

Moreover, in view of (21) and Lemmas 5 and 6, we have that, for any $\boldsymbol{\sigma}_f \in \widehat{\Sigma}(x)$,

$$\eta \circ \alpha_2^{-1}(V(x)) \leq \eta(|x|_{\mathscr{A}}) \leq |\boldsymbol{\sigma}_f|^2. \tag{36}$$

By defining $\alpha_3 := \eta \circ \alpha_2^{-1} \in \mathcal{K}_\infty$, (33a) stems from (35) and (36).

Proof of (33b). We split the analysis in two cases.

First, let $i \in \mathscr{V}$, $x \in D_i$ and $x^+ = g_i(x)$ as in Lemma 2. In view of the equality in (6) and the definition of V_{ij} in (20), we have $V_{ij}(x^+) = \int_0^{\theta_j^+ - \theta_i^+ + 2q_{ij}^+\pi} \sigma(\mathrm{sat}_{\pi+\delta}(s))ds = \int_0^{\theta_j - \theta_i + 2q_{ij}\pi} \sigma(\mathrm{sat}_{\pi+\delta}(s))ds = V_{ij}(x)$, and thus $V(x^+) = \sum_{(i,j)\in\mathscr{E}} V_{ij}(x^+) = \sum_{(i,j)\in\mathscr{E}} V_{ij}(x) = V(x)$.

Second, let $(i, j) \in \mathscr{E}$, $x \in D_{ij}$ and $x^+ \in G_{ij}(x)$ as in Lemma 1. In view of item a) of Property 1,

$$V_{ij}(x) = \int_0^{|\theta_j - \theta_i + 2q_{ij}\pi|} \sigma(\mathrm{sat}_{\pi+\delta}(s))ds. \tag{37}$$

On the other hand, in view of (4a), (4b) and Lemma 1, $|\theta_j^+ - \theta_i^+ + 2q_{ij}^+\pi| = |\theta_j - \theta_i + 2q_{ij}^+\pi| < \pi + \delta \leq |\theta_j - \theta_i + 2q_{ij}\pi|$, because $x \in D_{ij}$. Consequently, in view of (4a) and item b) of Property 1 $V_{ij}(x^+) = \int_0^{|\theta_j^+ - \theta_i^+ + 2q_{ij}^+\pi|} \sigma(\mathrm{sat}_{\pi+\delta}(s))ds < \int_0^{|\theta_j - \theta_i + 2q_{ij}\pi|} \sigma(\mathrm{sat}_{\pi+\delta}(s))ds = V_{ij}(x)$.

On the other hand, from the definition of G_{ij} in (4b), $V_{uv}(x^+) = V_{uv}(x)$ for any $(u, v) \neq (i, j) \in \mathscr{E}$. Therefore $V(x^+) - V(x) = V_{ij}(x^+) - V_{ij}(x) < 0$, since the arguments of all the other elements of the summation in (19) do not change. ■

Based on Lemma 9, we can now prove Proposition 2.

Proof of Proposition 2: Item (ii) of Proposition 2 is a direct consequence of (33b) in Lemma 9. To prove item (i) of Proposition 2 we exploit the fact that, in view of (Della Rossa, 2020, Lemma 2.23) and V being non pathological, for each solution x to (8), for all $j \in \{0, \ldots, J\}$ and almost all $t \in [t_j, t_{j+1}]$ in $\mathrm{dom}\, x$, $\frac{dV(x(t,j))}{dt} \in \dot{\overline{V}}_F(x(t, j))$. Hence, as a consequence, $\frac{d}{dt} V(x(t, j)) \leq -\kappa\underline{\lambda}\alpha_3(V(x(t, j))) + c\overline{\omega}$, thus concluding the proof. ■

8.3. Proof of Proposition 3

Paralleling Section 8.2, we establish via the next lemma geometric properties of V that can be used, together with Lemma 5 and Proposition 4, to show the trajectory-based result of Proposition 3.

Lemma 10. *If σ is discontinuous at the origin, then there exist $\mu \in \mathbb{R}_{>0}$ independent of $\overline{\omega}$ in* (14) *and $\kappa^\star > 0$ such that for each $\kappa > \kappa^\star$*

$$\sup \dot{\overline{V}}_F(x) \leq -\frac{1}{2}\kappa\underline{\lambda}\mu^2, \qquad \forall x \in C \setminus \mathscr{A}, \tag{38a}$$

$$\Delta V(x) := \sup_{g \in G(x)} V(g) - V(x) \leq 0, \qquad \forall x \in D. \tag{38b}$$

□

Proof: We only prove (38a), as (38b) follows from the same arguments as those proving (33b) in Proposition 2. For each $x \in C \setminus \mathscr{A}$ and each $f \in F(x)$, we may proceed as in (34) and then exploit from Lemma 7 that,

$$\sup \dot{\overline{V}}_F(x) \leq -\kappa \underline{\lambda} \mu^2 + c\overline{\omega}. \tag{39}$$

By selecting $\kappa \geq \kappa^\star = \frac{2c\overline{\omega}}{\underline{\lambda}\mu^2}$, (39) yields $\sup \dot{\overline{V}}_F(x) \leq -\frac{1}{2}\kappa\underline{\lambda}\mu^2$, which proves (38a). ■

Based on Lemma 10, we are now ready to prove Proposition 3.

Proof of Proposition 3: Item (ii) of Proposition 3 is a direct consequence of (38b) in Lemma 10. In view of (Della Rossa, 2020, Lemma 2.23) and V being non pathological, for each solution x to (8), for all $\mathrm{j} \in \{0, \dots, J\}$ and almost all $\mathrm{t} \in [\mathrm{t}_\mathrm{j}, \mathrm{t}_{\mathrm{j}+1}]$ in $\mathrm{dom}\, x$, $\frac{dV(x(\mathrm{t},\mathrm{j}))}{d\mathrm{t}} \in \dot{\overline{V}}_F(x(\mathrm{t},\mathrm{j}))$. Hence, as a consequence, $\frac{d}{d\mathrm{t}} V(x(\mathrm{t},\mathrm{j})) \leq -\frac{1}{2}\kappa\underline{\lambda}\mu^2$, whenever $x(\mathrm{t},\mathrm{j}) \notin \mathscr{A}$, thus proving item (i) of Proposition 3 which concludes the proof. ■

9. Conclusions

We presented a cyber-physical hybrid model of leaderless heterogeneous first-order oscillators, where global uniform asymptotic and/or finite-time synchronization is obtained in a distributed way via hybrid coupling. More specifically we establish that the synchronization set for the proposed model enjoys uniform asymptotic practical stability property. Thanks to the mild requirements on the coupling function, the stability result was strengthened to a prescribed finite-time property when the coupling function is discontinuous at the origin. Finally, we proved a useful statement on scalar non-pathological functions, exploited here for the non-smooth Lyapunov analysis in our main theorems. We believe that this work demonstrates the potential of hybrid systems theoretical tools to overcome the fundamental limitations of continuous-time systems.

Future extensions of this work include addressing graphs with cycles (not trees) and investigating the case with leaders as done for a second-order Kuramoto model in (Bosso et al. (2021a)). Additional challenges may include studying the converse problem of globally de-synchronizing the network (Franci et al. (2012)) via hybrid approaches.

Acknowledgement. The authors would like to thank Matteo Della Rossa and Francesca Maria Ceragioli for useful discussions about the results of Section 8.1, Elena Panteley for useful discussions and suggestions given during the preparation of the manuscript, and the reviewers of the submission, which allowed us, through their comments, to improve the overall quality of the work.

A. Appendix

Proof of Lemma 1: Let $(i,j) \in \mathscr{E}$, $x \in D_{ij}$ and x^+ satisfies (4b). Then, $\theta^+ = \theta$ while $q^+ \in \{-1,0,1\}^m$ in view of (4). Thus, $x^+ \in X$ and the first part of the statement is proved. Let $\Delta\theta_{ij} := \theta_j - \theta_i$, so that $\theta_j - \theta_i + 2q_{ij}\pi = \Delta\theta_{ij} + 2q_{ij}\pi$. Since $x^+ \in X$, by definition of X in (3), $|\Delta\theta_{ij}| < 2\pi + 2\delta$.

We now prove that $|\Delta\theta_{ij}^+ + 2q_{ij}^+\pi| = |\Delta\theta_{ij} + 2q_{ij}^+\pi| < \pi + \delta$ by exploiting the fact that $q_{ij}^+ = h^* \in \underset{h\in\{-1,0,1\}}{\mathrm{argmin}} |\Delta\theta_{ij} + 2h\pi|$ according to (4c), and splitting the analysis in five cases.

a) $\Delta\theta_{ij} \in (-\pi, \pi)$. Then, the minimizer is $h^* = 0$ and $|\Delta\theta_{ij} + 2h^*\pi| < \pi < \pi + \delta$.

b) $\Delta\theta_{ij} = \pi$. Then, the minimizer is $h^* \in \{-1, 0\}$ and $|\Delta\theta_{ij} + 2h^*\pi| \leq \pi < \pi + \delta$.

c) $\Delta\theta_{ij} = -\pi$. This case is identical to the previous one by changing all the signs, therefore $h^* \in \{0, 1\}$ and $|\Delta\theta_{ij} + 2h^*\pi| \leq \pi < \pi + \delta$.

d) $\Delta\theta_{ij} \in (\pi, 2\pi + 2\delta]$. Then, the minimizer is $h^* = -1$ and $\Delta\theta_{ij} + 2h^*\pi \in (-\pi, 2\delta]$, which implies $|\Delta\theta_{ij} + 2h^*\pi| < \pi + \delta$, since $\max(2\delta, \pi) < \pi + \delta$.

e) $\Delta\theta_{ij} \in [-2\pi - 2\delta, -\pi)$. In this case, the minimizer is $h^* = 1$ and $\Delta\theta_{ij} + 2h^*\pi \in [-2\delta, -\pi)$, which implies $|\Delta\theta_{ij} + 2h^*\pi| < \pi + \delta$, since $2\delta < \pi + \delta$.

Hence, we obtain, in view of all the previous cases, $|\theta_j^+ - \theta_i^+ + 2q_{ij}^+\pi| \leq \max(2\delta, \pi) < \pi + \delta$ thus concluding the proof since we have arbitrarily selected $(i,j) \in \mathscr{E}$. ■

Proof of Lemma 2: Let $i \in \mathscr{V}$, $x \in D_i$ and $x^+ = g_i(x)$. Let $(u,v) \in \mathscr{E}$, in view of (5), if $u \neq i$ and $v \neq i$ the first equality in (6) trivially holds. If $u = i$, then we have $\theta_v^+ - \theta_u^+ + 2q_{uv}^+\pi = \theta_v - \theta_u + \mathrm{sign}(\theta_u)2\pi + 2(q_{uv} - \mathrm{sign}(\theta_u))\pi = \theta_v - \theta_u + 2q_{uv}\pi$. Similarly, we obtain for $v = i$ that $\theta_v^+ - \theta_u^+ + 2q_{uv}^+\pi = \theta_v - \theta_u + 2q_{uv}\pi$, thus proving the first equality in (6). On the other hand, in view of (5b), $|\theta_i^+| = \pi - \delta < \pi + \delta$. Thus, all the elements of (6) are proved.

Let us now prove that $x^+ \in X$. In particular, we need to make sure that $q^+ \in \{-1,0,1\}^m$. For any $j \neq i \in \mathscr{V}$ we have that $\theta_j^+ = \theta_j$ and $|\theta_i^+| = \pi - \delta$ in view of (5b). Moreover, if j is such that $(i,j) \in \mathscr{E}$, then from (4a), (5d) we prove next that $q_{ij} \neq -\mathrm{sign}(\theta_i)$. Indeed, if $q_{ij} = -\mathrm{sign}(\theta_i)$ then we would have $|\theta_j - \theta_i + 2q_{ij}\pi| = \left|\theta_j - \mathrm{sign}(\theta_i)|\theta_i| - \mathrm{sign}(\theta_i)2\pi\right| = \left|\theta_j - \mathrm{sign}(\theta_i)(3\pi + \delta)\right| \geq 2\pi > \pi + \delta$, meaning that $x \in \mathrm{int}(D_{ij})$ and consequently $x \notin D_i$. Thus, $q_{ij} \neq -\mathrm{sign}(\theta_i)$ and, in view of (5c), we obtain $q_{ij}^+ \in \{0, -\mathrm{sign}(\theta_i)\}$. With a similar reasoning, we conclude that if j is such that $(j,i) \in \mathscr{E}$ then we must have $q_{ji} \neq \mathrm{sign}(\theta_i)$, implying that $q_{ji}^+ \in \{0, \mathrm{sign}(\theta_i)\}$ in view of (5c). Hence, $x^+ \in X$. ■

References

Acebron, J.A., Bonilla, L.L., Vicente, C.J.P., Ritort, F., Spigler, R., 2005. The Kuramoto model: A simple paradigm for synchronization phenomena. Reviews of Modern Physics 77, 137–185.

Aeyels, D., Rogge, J.A., 2004. Existence of partial entrainment and stability of phase locking behavior of coupled oscillators. Progress of Theoretical Physics 112, 921–942.

Alagoz, B., Kaygusuz, A., Karabiber, A., 2012. A user-mode distributed energy management architecture for smart grid applications. Energy 44, 167–177.

Anandan, N., George, B., 2017. A wide-range capacitive sensor for linear and angular displacement measurement. IEEE Transactions on Industrial Electronics 64, 5728–5737.

Aokii, T., 2015. Self-organization of a recurrent network under ongoing synaptic plasticity. Neural Networks 62, 11–19.

Bacciotti, A., Ceragioli, F., 1999. Stability and stabilization of discontinuous systems and nonsmooth Lyapunov functions. ESAIM: Control, Optimisation and Calculus of Variations 4, 361–376.

Bacciotti, A., Ceragioli, F., 2003. Nonsmooth optimal regulation and discontinuous stabilization. Abstract and Applied Analysis 2003, 1159–1195.

Bai, H., Arcak, M., Wen, J., 2011. Cooperative control design: a systematic, passivity-based approach. Springer Science & Business Media.

Baldoni, R., Corsaro, A., Querzoni, L., Scipioni, S., Tucci-Piergiovanni, S., 2007. An adaptive coupling-based algorithm for internal clock synchronization of large scale dynamic systems, in: OTM Confederated International Conferences "On the Move to Meaningful Internet Systems", Springer. pp. 701–716.

Bertollo, R., Panteley, E., Postoyan, R., Zaccarian, L., 2020. Uniform global asymptotic synchronization of Kuramoto oscillators via hybrid coupling, in: IFAC World Congress, pp. 5819–5824.

Bosso, A., Azzollini, I.A., Baldi, S., Zaccarian, L., 2021a. Adaptive hybrid control for robust global phase synchronization of Kuramoto oscillators. HAL, Also submitted for publication to the IEEE Transactions on Automatic Control hal-03372616, version 1.

Bosso, A., Azzollini, I.A., Baldi, S., Zaccarian, L., 2021b. A hybrid distributed strategy for robust global phase synchronization of second-order Kuramoto oscillators, in: IEEE Conference on Decision and Control, pp. 1212–1217.

Chopra, N., Spong, M.W., 2009. On exponential synchronization of Kuramoto oscillators. IEEE Transactions on Automatic Control 54, 353–357.

Clarke, F., 1990. Optimization and Nonsmooth Analysis. Classics in Applied Mathematics vol. 5, SIAM.

Coraggio, M., DeLellis, P., di Bernardo, M., 2020. Distributed discontinuous coupling for convergence in heterogeneous networks. IEEE Control Systems Letters 5, 1037–1042.

Cucuzzella, M., Trip, S., De Persis, C., Cheng, X., Ferrara, A., van der Schaft, A., 2018. A robust consensus algorithm for current sharing and voltage regulation in DC microgrids. IEEE Transactions on Control Systems Technology 27, 1583–1595.

Cumin, D., Unsworth, C.P.A., 2007. Generalising the Kuramoto model for the study of neuronal synchronisation in the brain. Physica D: Nonlinear Phenomena 226, 181–196.

De Persis, C., Frasca, P., 2013. Robust self-triggered coordination with ternary controllers. IEEE Transactions on Automatic Control 58, 3024–3038.

Della Rossa, M., 2020. Non-Smooth Lyapunov Functions for Stability Analysis of Hybrid Systems. PhD Thesis, University of Toulouse, France.

Della Rossa, M., Goebel, R., Tanwani, A., Zaccarian, L., 2021. Piecewise structure of Lyapunov functions and densely checked decrease conditions for hybrid systems. Mathematics of Control, Signals, and Systems 33, 123–149.

Della Rossa, M., Tanwani, A., Zaccarian, L., 2022. Non-pathological ISS-Lyapunov functions for interconnected differential inclusions. IEEE Transactions on Automatic Control 67, 3774–3789.

Dörfler, F., Bullo, F., 2012. Synchronization and transient stability in power networks and nonuniform Kuramoto oscillators. SIAM Journal on Control and Optimization 50, 1616–1642.

Dörfler, F., Bullo, F., 2014. Synchronization in complex networks of phase oscillators: A survey. Automatica 50, 1539–1564.

Dörfler, F., Bullo, F., 2011. On the critical coupling strength for Kuramoto oscillators, in: American Control Conference, pp. 3239–3244.

Forrester, D.M., 2015. Arrays of coupled chemical oscillators. Scientific Reports 5.

Franci, A., Chaillet, A., Panteley, E., Lamnabhi-Lagarrigue, F., 2012. Desynchronization and inhibition of Kuramoto oscillators by scalar mean-field feedback. Mathematics of Control, Signals, and Systems 24, 169–217.

Giraldo, J., Mojica-Nava, E., Quijano, N., 2019. Synchronisation of heterogeneous Kuramoto oscillators with sampled information and a constant leader. International Journal of Control 92, 2591–2607.

Godsil, C., Royle, G., 2001. Algebraic Graph Theory. Springer.

Goebel, R., Sanfelice, R.G., Teel, A.R., 2012. Hybrid Dynamical Systems: modeling, stability, and robustness. Princeton University Press.

Hájek, O., 1979. Discontinuous differential equations, I. Journal of Differential Equations 32, 149–170.

Jadbabaie, A., Motee, N., Barahona, M., 2004. On the stability of the Kuramoto model of coupled nonlinear oscillators, in: American Control Conference, pp. 4296–4301.

Jafarpour, S., Bullo, F., 2019. Synchronization of Kuramoto oscillators via cutset projections. IEEE Transactions on Automatic Control 64, 2830–2844.

Kiss, I.Z., 2018. Synchronization engineering. Current Opinion in Chemical Engineering 21, 1–9.

Kuramoto, Y., 1975. Self-entrainment of a population of coupled non-linear oscillators, in: International Symposium on Mathematical Problems in Theoretical Physics, Springer. pp. 420–422.

Leonard, N.E., Shen, T., Nabet, B., Scardovi, L., Couzin, I.D., Levin, S.A., 2012. Decision versus compromise for animal groups in motion. Proceedings of the National Academy of Sciences 109, 227–232.

Mauroy, A., Sepulchre, R., 2012. Contraction of monotone phase-coupled oscillators. Systems & Control Letters 61, 1097–1102.

Mayhew, C., Sanfelice, R., Teel, A., 2012a. On path-lifting mechanisms and unwinding in quaternion-based attitude control. IEEE Transactions on Automatic Control 58, 1179–1191.

Mayhew, C.G., R. G. Sanfelice, J. Sheng, M.A., Teel, A.R., 2012b. Quaternion-based hybrid feedback for robust global attitude synchronization. IEEE Transactions on Automatic Control 57, 2122–2127.

Mesbah, M., Egerstedt, M., 2010. Graph Theoretic Methods in Multiagent Networks. Princeton University Press.

Miller, R.B., Pachter, M., 1997. Maneuvering flight control with actuator constraints. Journal of Guidance, Control, and Dynamics 20, 729–734.

Oud, W.T., 2006. Design and experimental results of synchronizing metronomes, inspired by Christiaan Huygens. Master's Thesis, Eindhoven University of Technology.

Paley, D.A., Leonard, N.E., Sepulchre, R., Grunbaum, D., Parrish, J.K., 2007. Oscillator models and collective motion. IEEE Control Systems Magazine 27, 89–105.

Pandurangan, G., Robinson, P., Scquizzato, M., 2018. The distributed minimum spanning tree problem. Bulletin of EATCS 2.

Polyakov, A., 2011. Nonlinear feedback design for fixed-time stabilization of linear control systems. IEEE Transactions on Automatic Control 57, 2106–2110.

Rad, A., Jalili, M., Hasler, M., 2011. A lower bound for algebraic connectivity based on the connection-graph-stability method. Linear algebra and its applications 435, 186–192.

Reigosa, D., Fernandez, D., Gonzalez, C., Lee, S., Briz, F., 2018. Permanent magnet synchronous machine drive control using analog hall-effect sensors. IEEE Transactions on Industry Applications 54, 2358–2369.

Sanfelice, R.G., Copp, D., Nanez, P., 2013. A toolbox for simulation of hybrid systems in Matlab/Simulink: Hybrid Equations (HyEQ) Toolbox, in: Proceedings of the 16th International Conference on Hybrid Systems: Computation and Control, ACM. pp. 101–106.

Scholtes, S., 2012. Introduction to Piecewise Differentiable Equations. SpringerBriefs in Optimization, Springer.

Sepulchre, R., Paley, D.A., Leonard, N.E., 2007. Stabilization of planar collective motion: All-to-all communication. IEEE Transactions on Automatic Control 52, 811–824.

Song, Y., Wang, Y., Holloway, J., Krstić, M., 2017. Time-varying feedback for regulation of normal-form nonlinear systems in prescribed finite time. Automatica 83, 243–251.

Sontag, E.D., Wang, Y., 1995. On characterizations of the input-to-state stability property. Systems and Control Letters 24, 351–359.

Strogatz, S., 2003. Sync: The Emerging Science of Spontaneous Order. Hyperion, NY.

Strogatz, S.H., 2000. From Kuramoto to Crawford: Exploring the onset of synchronization in populations of coupled oscillators. Physica D: Nonlinear Phenomena 143, 1–20.

Tass, P.A., 2003. A model of desynchronizing deep brain stimulation with a demand-controlled coordinated reset of neural subpopulations. Biological Cybernetics 89, 81–88.

Valadier, M., 1989. Entraînement unilatéral, lignes de descente, fonctions Lipschitziennes non pathologiques. CRAS Paris 308, 241–244.

Wu, J., Li, X., 2018. Finite-time and fixed-time synchronization of Kuramoto-oscillator network with multiplex control. IEEE Transactions on Control of Network Systems 6, 863–873.

Xu, J., van den Boom, T.J.J., Schutter, B.D., Wang, S., 2017. Irredundant lattice representations of continuous piecewise affine functions. Automatica 70, 109–120.